JOURNAL OF GEOPHYSICAL RESEARCH, VOL. 108, NO. D2, 8236, doi:10.1029/2001JD001451, 2003

Long-range transport of continental plumes over the Pacific Basin: Aerosol physiochemistry and optical properties during PEM-Tropics A and B

K. G. Moore II, A. D. Clarke, V. N. Kapustin, and S. G. Howell
School of Ocean and Earth Sciences and Technology, University of Hawaii, Honolulu, Hawaii, USA

Received 1 November 2001; revised 27 April 2002; accepted 13 June 2002; published 3 January 2003.

[1] The Pacific Exploratory Mission Tropics (PEMT) A (1996) and B (1999) field campaigns occurred over a large area of the Pacific Basin and revealed the presence of "rivers" of continental outflow propagating into the remote marine atmosphere that were also supported by remote sensing and modeling efforts. Airborne measurements of both the coarse and fine mode aerosol during these campaigns provided assessment of the spatial variability in aerosol parameters (including optical properties and degree of internal versus external mixing) in continental plumes encountered over the Pacific Ocean. Large perturbations to the "pristine" marine atmosphere were observed. Most plumes were encountered in the Southern Hemisphere during PEMT A, while the opposite was observed during PEMT B. A variety of anthropogenic and natural sources for these continental plumes are suggested by the data, including biomass burning, urban/industrial emissions, and in the case of Asian outflow, dust storms. Aerosol size distributions (particularly for the refractory component) varied from one plume to another and most combustion-derived aerosol appeared to be an internal mix of a refractory soot-like constituent in a volatile matrix. Within the sampled plumes, size-resolved volatility suggested that this volatile matrix was relatively well neutralized, implying the presence of ammonia in the particle phase. The radiatively important single scatter albedo (ω) obtained from measured "dry" scattering and absorption coefficients ranged from approximately 0.88 (pollution with no coarse particles) to 0.94 (pollution and dust) in the free troposphere (FT) to 0.98 (pollution and sea salt) within the marine boundary layer (MBL). Vertical profiles often revealed more concentrated plumes aloft, typically situated in dry air with ambient relative humidity (RH) <40%, and much lower values of ω than in the underlying MBL. *INDEX TERMS:* 0305 Atmospheric Composition and Structure: Aerosols and particles (0345, 4801); 0360 Atmospheric Composition and Structure: Transmission and scattering of radiation; 0394 Atmospheric Composition and Structure: Instruments and techniques

Citation: Moore, K. G., II, A. D. Clarke, V. N. Kapustin, and S. G. Howell, Long-range transport of continental plumes over the Pacific Basin: Aerosol physiochemistry and optical properties during PEM-Tropics A and B, *J. Geophys. Res.*, *108*(D2), 8236, doi:10.1029/2001JD001451, 2003.

1. Introduction

[2] During the past 20 years various experiments in remote regions have revealed combustion emissions present even in supposedly pristine environments. These include the Arctic and Antarctic [*Schnell*, 1984; *Heintzenberg*, 1982] and the remote south Atlantic [*Andreae et al.*, 1984; *Clarke*, 1989] and Pacific [*Clarke*, 1989]. Recent aircraft experiments have revealed plumes and layers aloft generally derived from anthropogenic emissions, including urban/industrial pollution and biomass burning. These field campaigns have occurred at a variety of locations, had different distances from sources, and had different objectives/instrumentation. The following two paragraphs contain a sampling of recent aircraft campaigns that have either intentionally or serendipitously encountered continental emissions over the oceans; the first paragraph lists those that measured primarily urban/industrial plumes, the second paragraph lists those that predominantly measured biomass burning emissions.

[3] The Aerosol Characterization Experiment (ACE 1) [*Bates et al.*, 1998] and (ACE 2) [*Raes et al.*, 2000] had among its goals the quantification of the chemical and physical processes that control the properties and evolution of aerosol fields relevant to radiative forcing and climate. Both ACE 1 and ACE 2 were relatively remote from continental sources. ACE 2 occurred in the subtropical northeast Atlantic during 1997 and was influenced by urban emissions from Europe and occasionally dust outbreaks from the Saharan desert. The Tropospheric Aerosol Radiative Forcing Observational Experiment (TARFOX) [*Russell*

0148-0227/03/2001JD001451$09.00

et al., 1999a] studied the aerosol effects on climate change and occurred over the eastern seaboard of the United States during 1996. It sampled primarily urban/industrial emissions that are responsible for the regional haze frequently observed during the summer in this region. The Atlantic Stratocumulus Transition Experiment (ASTEX) [*Huebert et al.*, 1996] occurred in the summer of 1992 over the northeast Atlantic basin. It also periodically sampled air masses that were continentally influenced (urban emissions from Europe and African dust) [*Clarke et al.*, 1997].

[4] The Indian Ocean Experiment (INDOEX) [*Ramanathan et al.*, 2001] occurred during 1999 over the tropical Indian Ocean and investigated the climate effects and aerosol properties associated with the anthropogenic haze that emanates from India and South East Asia during the dry monsoon season. This haze has a strong biomass-burning component, although urban/industrial emissions are also present. INDOEX sampled both relatively close to the primary source region (India) and at some distance as well. ACE 1 took place in 1995 over the southern Pacific basin south of Australia in air that was relatively unperturbed by continental emissions. However, several "aged" biomass plumes were sampled [*Blake et al.*, 1999; *Posfai et al.*, 1999], particularly in the south central tropical Pacific atmosphere on the transit flights to this location. The Smoke, Clouds, Aerosols, Radiation-Brazil (SCAR-B) [*Kaufman et al.*, 1998] field campaign was designed to study the smoke, aerosols, and trace gases from biomass burning and their climactic effects and took place directly over/within the source region (the Brazilian rain forest and grasslands) during 1995. Two experiments took place concurrently during 1992 to study biomass-burning emissions from South America and southern Africa. These were the Southern Africa Fire-Atmosphere Research Initiative (SAFARI-92) [*Lindesay et al.*, 1996] and the Transport and Atmospheric Chemistry Near the Equator-Atlantic (TRACE-A) [*Fishman et al.*, 1996] projects. SAFARI-92 occurred directly over the southern Africa source region while TRACE-A studied South American and African outflow into the tropical south Atlantic atmosphere.

[5] However, few airborne observations exist for the extensive Pacific Basin and large uncertainties remain in the impacts of these plumes on the chemical and optical properties of the atmosphere. Recent model studies indicate that it is important to identify and characterize the aerosol component of these emission plumes because of their potential impact on global atmospheric chemistry and climate, including regional radiative forcing [*Penner et al.*, 1992; *Charlson et al.*, 1991] and cloud properties/precipitation [*Twomey et al.*, 1984; *Rosenfeld*, 1999; *Ackerman et al.*, 2000].

[6] One major goal of the Pacific Exploratory Mission Tropics (PEMT) A and B field campaigns was to study the influence of these emissions on the remote tropical Pacific atmosphere. PEMT A occurred during 1996 from September through October during a climatologically representative year [*Fuelberg et al.*, 1999] while PEMT B occurred during 1999 from February through April during a La Nina event [*Fuelberg et al.*, 2001]. This vast region had not been sampled in great detail in the past [*Hoell et al.*, 1999; *Raper et al.*, 2001] and had been assumed to be representative of natural background conditions since it is remote from any significant anthropogenic sources. However, several extensive continental/combustion plumes were identified and their aerosol microphysical and optical properties were characterized.

[7] The aerosol parameters measured on board the P3-B aircraft (one of two aircraft in both experiments) include those necessary for radiative model inputs such as scattering and absorption coefficients, mass of aerosol chemical components (sulfates, soot, etc.), size distributions for the various components, degree of internal versus external mixing, and spatial distribution of absorbing and nonabsorbing aerosols [*Heintzenberg et al.*, 1997; *NRC*, 1996]. The optical properties of aerosols are described by their scattering and absorption coefficients. These are typically combined into the single scatter albedo (ω), which is defined as the ratio of scattering coefficient (σ_{sp}) to the sum of scattering and absorption (σ_{ap}) coefficients ($\omega = \sigma_{sp}/(\sigma_{sp} + \sigma_{ap})$). Few large-scale experiments have been conducted where all of the above parameters have been measured simultaneously, especially in the remote troposphere.

2. Aerosol Instrumentation and Measurements

[8] Continental aerosol plumes often have elevated concentrations of condensation nuclei (CN) aerosol with a variety of compositions, including sulfates, nitrates, dust, carbonaceous aerosol and soot. These aerosols are typically found in size ranges that dominate aerosol light scattering and absorption [*NRC*, 1996] with enhanced accumulation mode aerosol (diameters between 0.1 and 1.0 μm). Size distributions measured at ambient and elevated temperatures (i.e., 150° and 300°C) can also reveal information on the volatile (sulfates, nitrates, etc.) and refractory (soot, dust, etc.) components [*Clarke*, 1991; *Smith and O'Dowd*, 1996] as well as their state of mixing (internal versus external) [*Clarke et al.*, 1997]. Such thermal analysis will form the basis of several measurements described below. An enhanced concentration of refractory condensation nuclei (RCN) remaining after heating the ambient aerosol to high temperatures is usually a very good indicator of the presence of surface derived aerosol such as soot, sea salt, and/or dust [*Clarke*, 1991; *Clarke et al.*, 2001]. However, utilizing elevated concentrations of aerosol (either ambient or the refractory component) alone to identify combustion plumes can be misleading since dilution of the air mass, removal processes, and other factors can reduce the concentrations. A less variable parameter for identifying combustion plumes is the ratio of unheated CN to RCN (referred to henceforth as the RCN ratio). Significant enhancements of this ratio above background values (in the absence of sea salt or dust) usually indicate combustion aerosol [*Clarke et al.*, 1997].

[9] Aircraft aerosol instrumentation for the two experiments provided assessment of these and related aerosol properties. Table 1 identifies and lists the aerosol instrumentation utilized on the P-3B during the two field campaigns and relevant measurement parameters. The combined data sets presented in this paper are available in the NASA data archive (ftp://ftp-gte.larc.nasa.gov/pub) and measurement techniques (including gas phase and meteorological parameters) are described by *Hoell et al.* [1999] and *Raper et al.* [2001] (for PEMT A and B, respectively). The appropriate references are contained therein.

Table 1. Aerosol Instrumentation

Instrument	Measurement	Size Range, μm	Instrument RH, %	Averaging Time, s	λ, nm
2 TSI 3760 CN counters (for PEMT-A)	CN concentrations (@40 and 300°C)	0.012–3.0 (nominal)	NA	15	NA
2 TSI 3010 CN counters (for PEMT-B)	CN concentrations (@40 and 300°C)	0.010–3.0 (nominal)	NA	10	NA
1 TSI 3025 UCN counter (both)	UCN concentrations (@40°C)	0.003–3.0	NA	10 for PEMT-B, 15 for PEMT-A	NA
1 custom TRDMA (PEMT-A)	Size distributions (@40, 150, and 300°C)	0.007–0.20	5–40	90	NA
1 TSI 3934 Long DMA (PEMT-B)	Size distributions (@40, 150, and 300°C)	0.010–0.28	5–40	90	NA
1 custom LOPC (both)	Size distributions (@40, 150, and 300°C)	0.148–7.5 (PEMT-A), 0.100–4.5 (PEMT-B)	5–40	Typically 60–120	NA
1 TSI 3076 3-λ nephelometer (both)	Aerosol total scattering and backscattering coefficients	Dp ≤ 7.5	10–50	30 (horizontal legs for computing ω)	450, 550, 700
1 RR PSAP (both)	Aerosol absorption coefficient	Dp ≤ 7.5	10–50	Horizontal legs	565

[10] Some details of our aerosol measurements are listed below.

2.1. CN Concentrations

[11] During both experiments, one CN counter measured aerosol concentrations at ambient temperature while another measured refractory CN (RCN) after heating the sample to 300°C (see Table 1 for the PEMT A and B CN counter cut sizes). RCN are generally surface derived soot, dust, or sea-salt. At altitudes above the inversion (~1.5 km) the latter are uncommon. The difference between the ultrafine CN (UCN) counter ($D_p \geq 0.003$ μm) and the unheated CN counter was used to identify "ultrafine" (UF) nuclei with diameters between 3 and 12 nm (PEMT A) and between 3 and 10 nm (PEMT B), usually indicative of recent particle formation. The CN, RCN, and UF concentrations throughout this paper have been corrected to standard temperature and pressure (STP, similar to a mixing ratio) using a standard pressure of 1013 mbar and temperature of 298.15 K.

2.2. Aerosol Size Distributions

[12] Number size distributions for the larger aerosol (see Table 1 for size ranges) were measured using a custom Laser Optical Particle Counter (LOPC; PMS, Boulder, Co) [*Clarke*, 1991]. The difference in the size ranges for the two experiments is due to a change in the instrument electronics. During PEMT A, a Radial Differential Mobility Analyzer (RDMA) [*Zhang et al.*, 1995] was utilized for measuring size distributions for the smaller aerosol (see Table 1) while a Long DMA (LDMA, TSI 3934) was used during PEMT B. OPC size distributions were measured "dry" (typically 20–40% relative humidity (RH)) after diluting the sample flow with dry air. DMA sizes were also for "dry" aerosol since the DMA operated with desiccated sheath air. Heated size distributions and associated volatility at 150°C and 300°C allowed inference of aerosol composition [*Clarke*, 1991; *Smith and O'Dowd*, 1996]. Heating to 150°C "cooks" off the acidic aerosol components (primarily sulfuric acid). If the distribution is relatively unchanged after heating to 150°C, the inference is that this aerosol is neutralized, presumably by the presence of ammonia in the particle phase. The "refractory" size distribution remaining in the accumulation mode ($0.1 \leq$ diam ≤ 1.0 μm) after heating the ambient aerosol to temperatures of 300°C ("cooking" off the sulfuric acid and sulfates) is often a useful indicator of combustion by-products and frequently attributed to soot [*Clarke*, 1991; *Smith and O'Dowd*, 1996]. OPC and DMA distributions have been combined in this paper and include a region of overlap between the two that generally shows agreement within ~10%. Size distributions were also corrected to STP conditions (with the exception of data presented in Figure 15).

2.3. Internal Versus External Mixing

[13] In addition, during PEMT-A the RDMA had the option of running in the TDMA mode (tandem DMA). This allowed us to select one size in the ambient distribution (often chosen to be the peak of the accumulation mode) and then heat that size to 300°C. The residual refractory aerosol was then scanned with the second RDMA and the resulting number/volume distributions were used to determine the degree of internal versus external mixing of the aerosol. Any shift to smaller sizes indicated the refractory aerosol was associated with a volatile constituent. The effective size of the refractory and volatile components can then be determined. The aerosol is considered internally mixed if the integral number is approximately conserved after heating [*Clarke*, 1991]. The degree of mixing within aerosols reveals features linked to the origin and evolution of the aerosol as well as potential differences in optical properties. Modeled optical properties can differ depending on whether one assumes an external or internal mixture of the soot and sulfate aerosols.

2.4. Aerosol Optical Properties

[14] The aerosol total hemispheric scattering and backscattering coefficients (see Table 1) were measured using a TSI 3076 integrating three-wavelength nephelometer [*Anderson et al.*, 1996b]. An impactor with an aerodynamic size cut of 1.0 μm was occasionally switched in-line during horizontal legs with the inlet of the nephelometer to separately determine the relative contribution to the scattering from all particles versus submicron particles. The measured scattering coefficients have been corrected for the illumination and truncation errors inherent in the instrument as per *Anderson et al.* [1996b].

[15] Absorption coefficients (see Table 1) for both field campaigns were measured by a particle/soot absorption photometer (PSAP) (Radiance Research, Seattle) and were averaged over entire horizontal legs. The scattering coefficients were also averaged over horizontal legs when used to calculate ω. *Bond et al.* [1999] have developed corrections for this instrument, which were applied to the measured absorption coefficients.

[16] Historically, aerosol light scattering and absorption coefficients have been reported as non-STP corrected values due to their use in column optical and radiative properties and comparison to satellite and ground remote sensing measurements. Therefore, these parameters were not converted to STP conditions in this paper.

2.5. "LAG" Chamber

[17] All of the above instrumentation sampled directly from the aerosol inlet, except for the DMAs. The DMAs normally operated with scan times of 90 s (for each temperature) in order to obtain a size distribution. At typical P-3B speeds (greater than 100 m/s), large variations in aerosol properties can occur over this time period. Therefore, a Lagged Aerosol Grab (LAG) chamber [*Clarke et al.*, 1998] was utilized to capture an air sample over a 20-s period that was then scanned by the DMAs sequentially at three temperatures.

2.6. RH Effects

[18] The size distributions (DMA and OPC) and optical properties (aerosol scattering from nephelometer and aerosol absorption from PSAP) were measured at instrument RH values (Table 1) that were less than ambient conditions. Size distributions were "dried" before measurement; distributions at ambient RH would be larger due to hygroscopic growth. How much larger depends on the aerosol composition, particle size, instrument RH, and ambient RH, but this growth can be modeled by using an appropriate aerosol growth factor [*Tang and Munkelwitz*, 1993; *Hagen et al.*, 1989]. Nephelometer measurements were not specifically "dried," but scattering coefficients were measured at RH values reflective of sample line conditions (less than ambient RH due to RAM heating and higher cabin temperatures). Ambient scattering coefficients (σ_{sp}) will be larger due to hygroscopic growth. The increase in σ_{sp} is not the same as the growth factor for the size distribution, however, since in addition to growing to larger sizes, the index of refraction of the aerosol will decrease due to the uptake of water. Humidification factors (f(RH)) allow for the correction of scattering coefficients from instrument RH to ambient conditions and have been measured in a variety of continental/combustion plumes, including during INDOEX [*Ramanathan et al.*, 2001], TARFOX [*Kotchenruther et al.*, 1999], and SCAR-B [*Kotchenruther and Hobbs*, 1998]. The PSAP sampled at approximately the same RH as the nephelometer (reflective of cabin conditions). There is currently some debate as to the effect of RH on measured absorption coefficients. Some authors [*Chylek et al.*, 1995] have suggested an enhancement of absorption due to liquid water "focusing" light on the underlying soot. However, some recent modeling studies [*Fuller et al.*, 1999] have revealed no such enhancement. The majority of results reported in this study were for free troposphere (FT) continental/combustion plumes sampled during PEMT A and B and the average ambient RH for all plumes was less than 40% (Figure 4 and Table 3). Therefore, corrections to size distributions and optical properties would be negligible (<5%) and have been ignored. The values of ω in this paper were reported as "dry" values (reflecting the lower RH in the instruments), but in actuality are reflective of ambient conditions (within the discussed FT plumes) in light of the above discussion.

2.7. Inlet Losses

[19] Inlet losses occur when sampling aerosol from aircraft, particularly for the largest particles (diameters > 3.0 μm). These losses will most affect the OPC size distributions and nephelometer scattering coefficients when coarse particles are present. Corrections based upon field studies [*Porter et al.*, 1992] have been applied to the OPC size distributions. Nephelometer data were not corrected for losses, but recent inlet tests (Passing Efficiency of a Low Turbulence Inlet (PELTI) experimental results, B. Huebert, personal communication) have indicated that even when particles larger than 3 μm are present, the corrections for scattering data are relatively small (<10%) for our group's inlet (solid diffuser, not the LTI). The majority of measurements discussed in this paper were sampled in the free troposphere (FT) and in the absence of coarse mode particles ($D_p \geq 1.0$ μm); therefore corrections to the measured scattering coefficients would be less than this. No inlet loss corrections were assumed/applied to absorption coefficients. This would only affect results when coarse mode dust aerosols (mildly absorbent) are present.

3. Observations

3.1. General Overview/Large-Scale Observations

[20] Figure 1 contains a map of the Pacific Basin and the flight tracks of the P3-B aircraft for PEMT A (flights 7–19, October and September 1996) and B (flights 4–19, March and April 1999). A complete description of the PEMT A and B field experiments (including dates of flights, instrument description, etc.) are given by *Hoell et al.* [1999] and *Raper et al.* [2001]. The flight tracks are color-coded to the STP corrected RCN concentrations for those portions of the flights above 1.5 km altitude, chosen to exclude marine boundary layer (MBL) data. Several regions of enhanced concentrations are discernible over a significant portion of the Pacific Basin. Region 2 (PEMT A) is located in the Eastern Pacific off South America with elevated RCN extending over 1500 km from the coast. Region 3 (PEMT A) is located in the Central Pacific in the vicinity of Tahiti. This region is over 4000 km from any continents and was anticipated to be among the "cleanest" regions sampled. However, enhanced RCN were observed from over 700 km northwest to 1500 km southeast of Tahiti (over 2000 km in extent). Region 4 (PEMT B) is located over the northern Pacific Basin to the northeast of the Hawaiian Islands and extends to the California coast (approximately 3000 km). These distances suggest the extent of these continental plumes and that a significant portion of the North and South Pacific basin was affected by continental emissions during the PEMT A and B field campaigns.

[21] In general, PEMT B exhibited less perturbed conditions than PEMT A (especially in the tropical Southern Hemisphere) as evidenced by the lower RCN values observed over much of the flight tracks. Here we select region 1 (PEMT B) as having aerosol and gas phase measurements most representative of background marine atmospheric conditions. These measurements will be utilized as a baseline for assessing the magnitude of the perturbation of continental plumes on "natural" conditions in the Pacific marine environment.

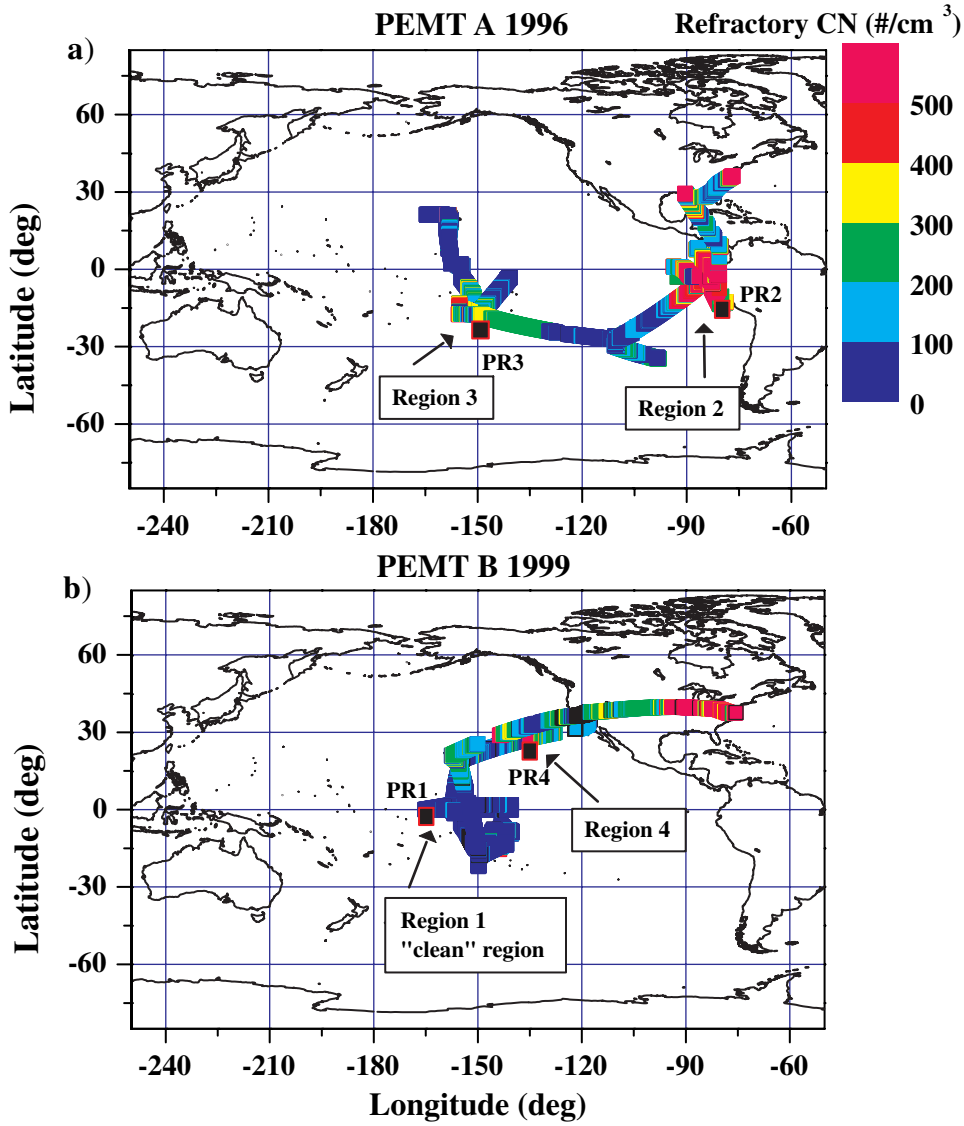

Figure 1. (a) The flight tracks of the P3-B are shown for PEMT A flights 7 through 19, color coded to STP corrected RCN concentrations (an aerosol combustion indicator). Two main regions of enhanced RCN are shown in the figure (region 2, South American coast, and region 3, Central Pacific). (b) Same as (a), but for PEMT B flights 4 through 19. Region 4 contains elevated RCN in the northern Central Pacific. Also shown is an area labeled region 1 that was chosen to represent the background (i.e., "clean") marine atmosphere. The location of vertical profiles discussed later for regions 1, 2, 3, 4 are labeled PR1, PR2, PR3, and PR4, respectively.

[22] Figure 2 shows the combined flight tracks as a function of latitude and altitude, color-coded to the RCN ratio. Higher ratios indicate a more refractory continental aerosol. Region 2 (Figure 2b) clearly exhibits higher RCN ratios in the FT from 2 to 6 km in altitude and extending from the equator to 10°S latitude. During PEMT B (region 4, Figure 2c), air masses with elevated RCN ratios in the FT were observed at most altitudes from 2 to 8 km and extending from 10°N to 35°N latitude. This enhancement was observed on flights through this region separated in time by over a month, indicating that such features were present over a similar timescale. Region 1 ("clean" equatorial region) is also shown in Figure 2c. Enhanced RCN ratios in the FT are observed in the Central Pacific (region 3, Figure 2a) as well from approximately 15 to 25°S latitude and from 2 to 6 km altitude.

[23] These figures represent a series of point measurements and do not convey the sinuous "river-like" structure mentioned previously. One really needs to have remote sensors/models to detect the large-scale structure of these plumes. For example, satellite images taken over the Northern Pacific during PEMT B (region 4) revealed dust and combustion aerosol plumes [*Clarke et al.*, 2001] emanating from the Asian continent several days prior to the P-3B sampling in region 4. Models for this same time period/region [*Clarke et al.*, 2001] captured the "river-like" structure associated with this plume. Lidar images from PEMT A showed two-dimensional cross sections through

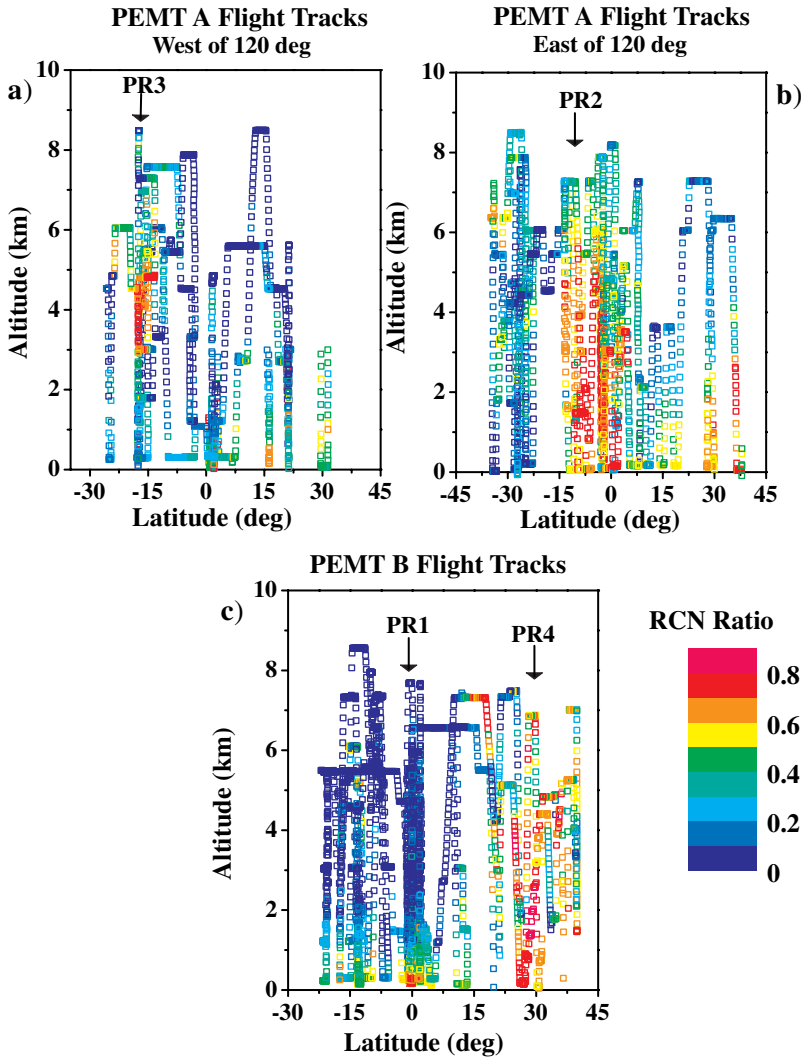

Figure 2. (a) RCN ratio as a function of altitude and latitude encompassing region 3 (west of 120°W longitude). (b) RCN ratio as a function of altitude and latitude for region 2 (east of 120°W longitude). (c) Region 4 (north Central Pacific) shows enhanced RCN ratio in the midlatitudes. Locations of PR1, PR2, PR3, and PR4 are shown on this figure as well.

the plumes sampled in region 3 (Central Pacific) [*Fuelberg et al.*, 1999; see *Journal of Geophysical Research* front cover: PEMT A first special section, 1999] and also demonstrated their "river-like" structure. While no satellite/lidar images or model results are in publication for region 2 (South American coast) during PEMT A, model results from TRACE A (Amazon basin biomass burning, September–October, 1992) showed plumes originating over the Amazon basin and occasionally spilling over the Andes into the Eastern Pacific troposphere [*Krishnamurti et al.*, 1996, Plates 7 and 8]. Later we will characterize the in-situ microphysical and optical properties of these plumes.

3.2. Backtrajectories/Source Regions

[24] In the previous section, the regions of elevated RCN and RCN ratio discussed were inferred to be combustion/continental in origin. While local sources for combustion plumes do exist in the remote Pacific (ship plumes and pollution from island chains), it is unlikely that any local source could perturb the Pacific FT on the large scales described above. Therefore, representative backtrajectories were utilized to confirm the continental origin of the plumes considered here.

[25] Figure 3a shows representative 10-day backtrajectories [*Fuelberg et al.*, 1999, 2001] for the selected FT combustion plumes and "clean" air mass referred to in the preceding section. In all four regions, rather large vertical excursions are evident and reveal the complicated "histories" of the respective air masses. The "clean" equatorial region 1 backtrajectory (Figures 3a and 3b) confirms that this air mass had not been over any continental regions within the past 10 days and allows for its characterization as "aged" marine air. At approximately 155°W longitude, the air parcel swings to the north toward the Inter-Tropical Convergence Zone (ITCZ, a convectively active region) where it rises in altitude significantly before subsiding and returning to its original latitude/altitude.

[26] A backtrajectory for the FT plume off South America (region 2, Figure 3c) suggests that the source for this plume was to the east from the South American continent. In fact,

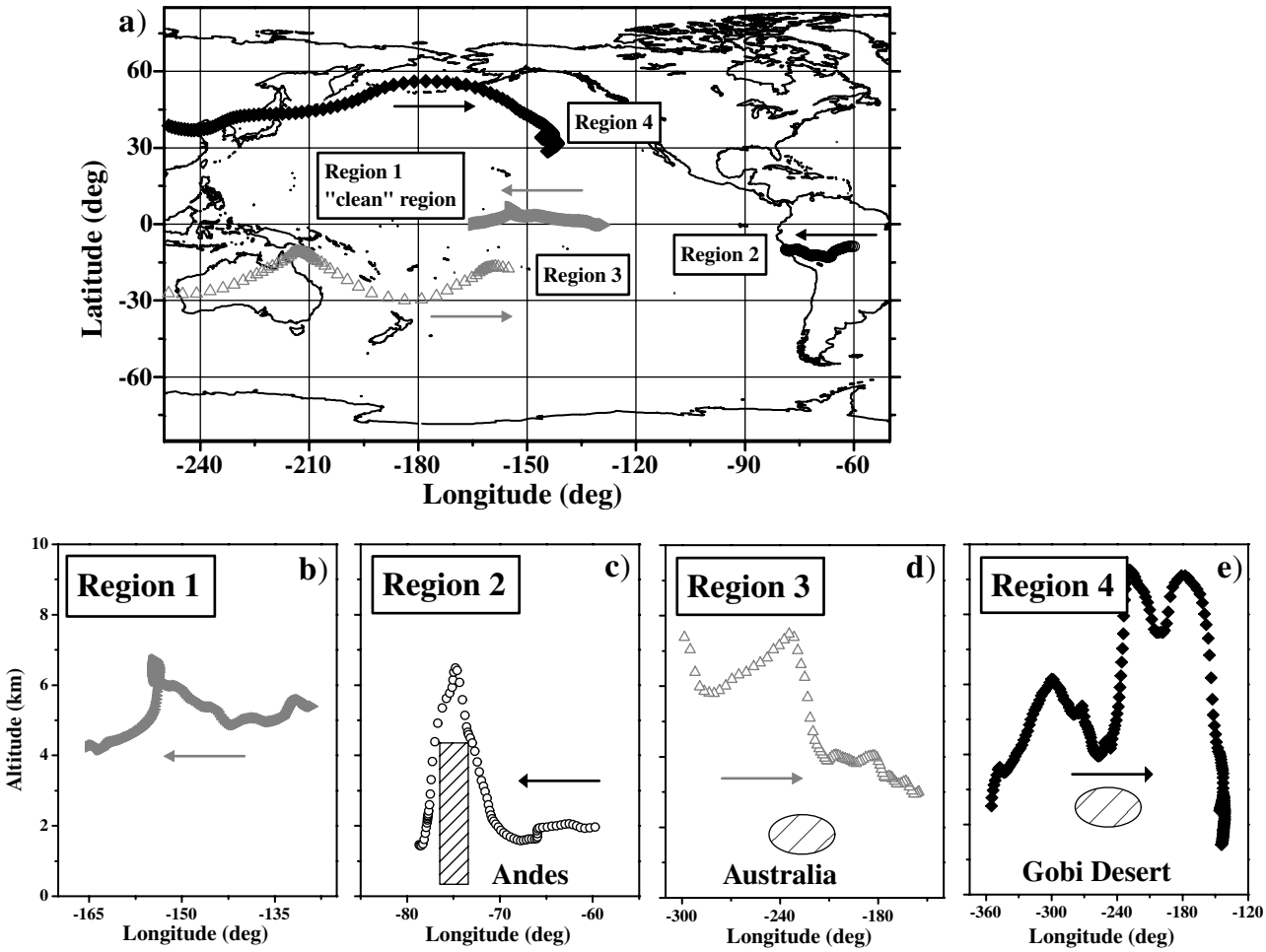

Figure 3. Backtrajectories for the FT plumes encountered in the three regions. The arrows show the general direction of motion of the respective air masses. (a) shows the sources for the four regions. (b) ''clean'' region 10 day backtrajectory as a function of longitude and altitude. Note the lack of continental influences in the previous 10 days. (c) Same as 10b, but for the region 2 FT biomass plume. Note the transit over the Andes. (d) Same as 10b, but for region 3. The air mass containing the plume has been subsiding from high altitudes throughout much of its history. (e) Same as 10b, but for region 4. This air mass descended to the surface over the Asian continent where it obtained its continental (combustion and dust) component and subsequently long-range transported over the northern Central Pacific.

this figure indicates the air parcel crossed over the Amazon basin (a known biomass burning region during the dry season) between 5 and 10 days prior to sampling before crossing over the Andes.

[27] The backtrajectory for region 3 in the South Pacific westerlies near Tahiti (Figure 3d) shows the FT plume (2 to 6 km) originated from the west, having passed over the Australian continent approximately 4 days earlier. However, 10 days before sampling, the air parcel passed over southeastern Africa. Both Australia and Africa have been linked to biomass burning during the austral spring (dry season). Regardless of the source, it is apparent from the figure that the plume was carried aloft and has been subsiding from much higher altitudes than where it was sampled.

[28] The backtrajectory shown in Figure 3e for the North Pacific westerly flow (region 4) is suggestive of an Asian source for this plume. The air parcel passed over the Gobi desert (approximately 110°E longitude, 40°N latitude, and 2 km altitude) 5 to 10 days prior to sampling at the aircraft location. The Gobi desert is a known source for Asian dust and dust storms are frequent in this region during spring in the Northern Hemisphere. The air parcel passed through cyclonic activity in the coastal regions of Asia after that, where it likely obtained a combustion component (from biomass burning and/or urban emissions).

[29] The four backtrajectories shown here were selected to be representative of the ''clean'' and continentally influenced air that arrived at the aircraft's location and altitude at the time of sampling. However, they are not representative of other air masses sampled at other altitudes in the various regions as will be made clear in the following sections.

3.3. Case Studies: Vertical Structure, Size Distributions, Volatility, and TDMA Results

[30] Figures 1 and 2 are suggestive of the vertical and spatial extent of aerosol plumes sampled during PEMT A and B and the extended temporal scales associated with the

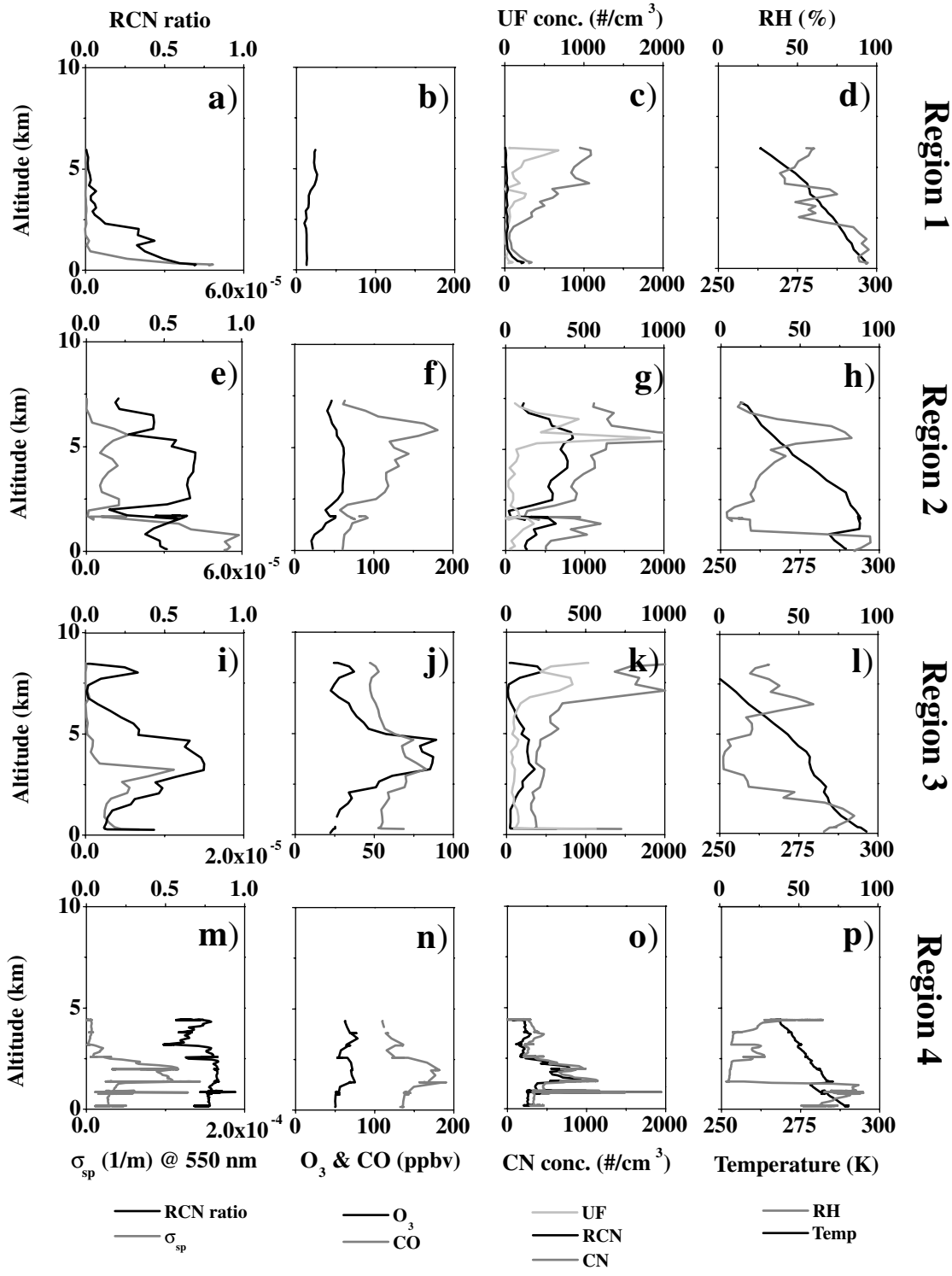

Figure 4. Vertical profile of various aerosol, gas phase, and meteorological variables for regions 1 through 4. Note the variety of scales. (a)–(d) are for the ''clean'' region (region 1, equatorial Central Pacific, PEMT B). (a) RCN ratio and scattering coefficient. (b) O_3 and CO concentrations. (c) CN, RCN, and UF concentrations. (d) ambient RH and Temperature. (e)–(h) are the same as (a)–(d), but for region 2 (South American coast, PEMT A). (i)–(l) are the same as (a)–(d), but for region 3 (Central Pacific, PEMT A). (m)–(p) are the same as (a)–(d), but for region 4 (north Central Pacific, PEMT B).

two experiments. The backtrajectories are consistent with continental sources for the various plumes. Detailed knowledge of the vertical distribution of aerosol properties and gas phase components within these plumes is desirable to assess their role in radiative forcing. Figure 4 plots various aerosol, meteorological, and gas phase properties as a function of altitude for a ''clean'' environment and three continentally perturbed regions. Vertical profiles of the

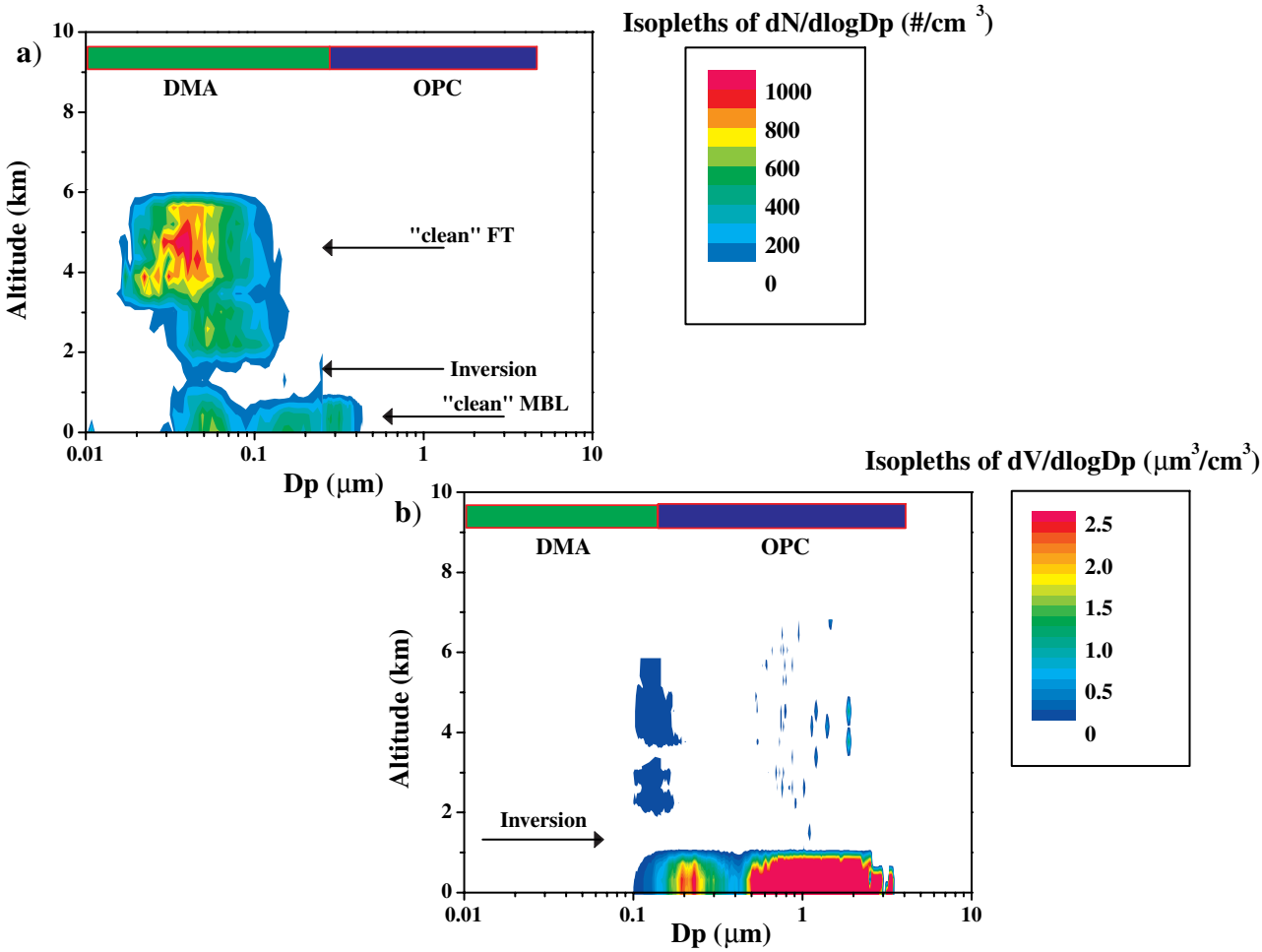

Figure 5. Vertical profile of aerosol size distributions for the "clean" region (region 1, equatorial Central Pacific, PEMT B). (a) Unheated number distributions color coded to dN/dlogDp (concentration). (b) Unheated volume distributions color coded to dV/dlogDp (volume).

unheated number and volume distributions are shown in Figures 5–8 and clearly demonstrate distinctions between "clean" air and the various combustion/continental plumes. The locations of these profiles (labeled PR1, PR2, PR3, and PR4 for profiles in regions 1, 2, 3, and 4, respectively) are indicated in Figures 1 and 2, and contained in Table 2. Also contained in Table 2 are the dates of these flights.

[31] The aerosol size distributions and associated size-resolved volatility at 150° and 300°C are shown in Figures 9–12 for representative altitudes and locations within the various regions and provide additional information as to the nature of the aerosol contained therein. TDMA volatility studies were utilized to assess the degree of internal versus external mixing within the aerosol sampled and, where available (none during PEMT B), are shown in Figures 9–12. Unfortunately, time constraints precluded the measurement of heated distributions and TDMA studies during actual vertical profiles. However, the distributions discussed in the following sections were sampled sufficiently proximal in both time and location to the vertical profiles to be considered representative. It should be noted that no adjustments to the OPC and DMA size distributions was made and that the relatively good agreement in the overlap portion of the distributions was as measured.

3.3.1. Region 1: PEMT B Flight 12 ("Clean/Aged" Maritime Air)

3.3.1.1. Vertical Structure

[32] Region 1 (Figure 1) is located in the equatorial central Pacific to the south of the ITCZ, is characterized by easterly flow at all altitudes sampled, and the back-trajectory from Figure 3a suggests no continental influence within the previous 10 days. The vertical profile labeled PR1 in Figure 1 was located at approximately 164°W and 0°N. The profile of aerosol scattering coefficient (Figure 4a) for the "clean" marine atmosphere shows very low values above 2 km (the FT) with the highest values found below 1 km altitude (the MBL) due to the presence of coarse mode (diameters $\geq$1.0 μm) sea salt. Between 1 and 2 km is a transition zone from the MBL to the FT (often referred to as the "buffer layer") with intermediate values of these properties. RCN concentrations (Figure 4c) are low and fairly constant in the FT; concentrations are highest in the MBL due to refractory sea salt. The RCN ratio (Figure 4a) is negligible in the "clean" FT reflecting the highly volatile nature of the aerosols typically found there. Within the

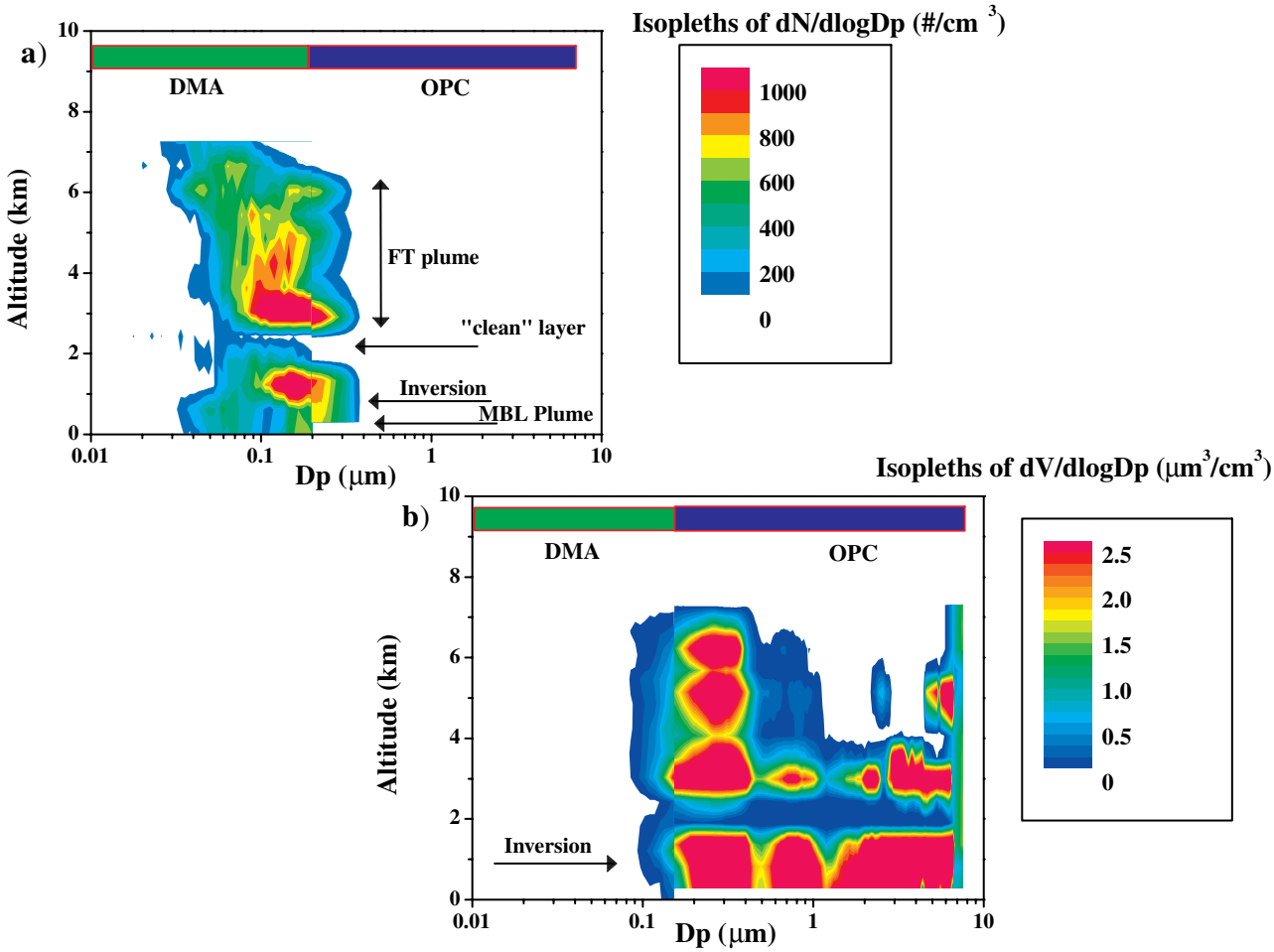

Figure 6. Same as Figure 2, but for region 2 (South American coast, PEMT A).

"buffer layer" and MBL, the RCN ratio is elevated from sea salt, not from combustion sources since aerosol light absorption was within the instrument detection limit ($<1.0 \times 10^{-7}$ m^{-1}, Table 3). Also, O_3 concentrations (Figure 4b) (Ridley, archive data) are fairly uniform throughout the entire profile and give no indication of combustion-influenced air (no CO data available for this profile).

[33] Unlike the surface derived RCN, the total CN and UF (particles with diameters between 3 and 12 nm) generally increased with altitude. The low scattering values and increasing volatile nuclei with height evident in Figures 4a and 4c is typical for the "clean" marine atmosphere [*Clarke et al.*, 1999]. The temperature profile (Figure 4d) exhibited very weak inversions at approximately 1, 2, and 4 km, while the ambient RH (Figure 4d) possessed more structure. There was a layer with higher RH values at ~5.8 km which coincided with peaks in CN and UF concentrations (and minima in RCN ratio, i.e., "clean"), most likely representing earlier cloud outflow at this altitude. This flight did take place in the vicinity of the Inter Tropical Convergence Zone (ITCZ), a feature in the tropical atmosphere where convective activity occurs on a regular basis [*Fuelberg et al.*, 2001]; the backtrajectory for this region (Figure 3b) is consistent with convection having influenced this air mass. The backtrajectory for the MBL air was very similar to the FT trajectory shown in Figures 3a and 3c (air mass came from the east and had not been over land in the last 10 days) except that at the far eastern end, the air mass came from the northeast in the typical trade wind pattern found in this area.

[34] Unheated number and volume distributions (combined from both the DMA and OPC) as a function of diameter versus altitude (and color coded to dN/dlogDp and dV/dlogDp, i.e., concentration) are shown in Figure 5. The results shown are similar to previous data for the remote marine atmosphere. The number distribution below 1 km altitude is bimodal as is expected for cloud-processed air in the MBL [*Hoppel et al.*, 1986]. At 3–6 km, the number distribution exhibits a peak at relatively small diameters (Dp $\approx$ 0.025 μm) with few particles having diameters $\geq$0.1 μm (the most "optically active" portion of the size distribution). The volume distributions within the MBL contain two modes: the accumulation mode aerosol ($0.1 \leq$ Dp ≤ 0.3 μm) and coarse mode sea salt (Dp ≥ 0.5 μm) typically found in the MBL. There is no significant volume observed aloft (typical for the "clean" marine FT).

3.3.1.2. Size Distributions and Volatility

[35] The volume and number distributions (at all three temperatures) for the "clean" MBL (~500m) and FT (~4 km) are shown in Figure 9. In the FT (Figure 9a), the unheated volume distribution is highly volatile (virtually none of the volume remains after heating the aerosol to 150°C). Two modes are clearly visible for the MBL aerosol

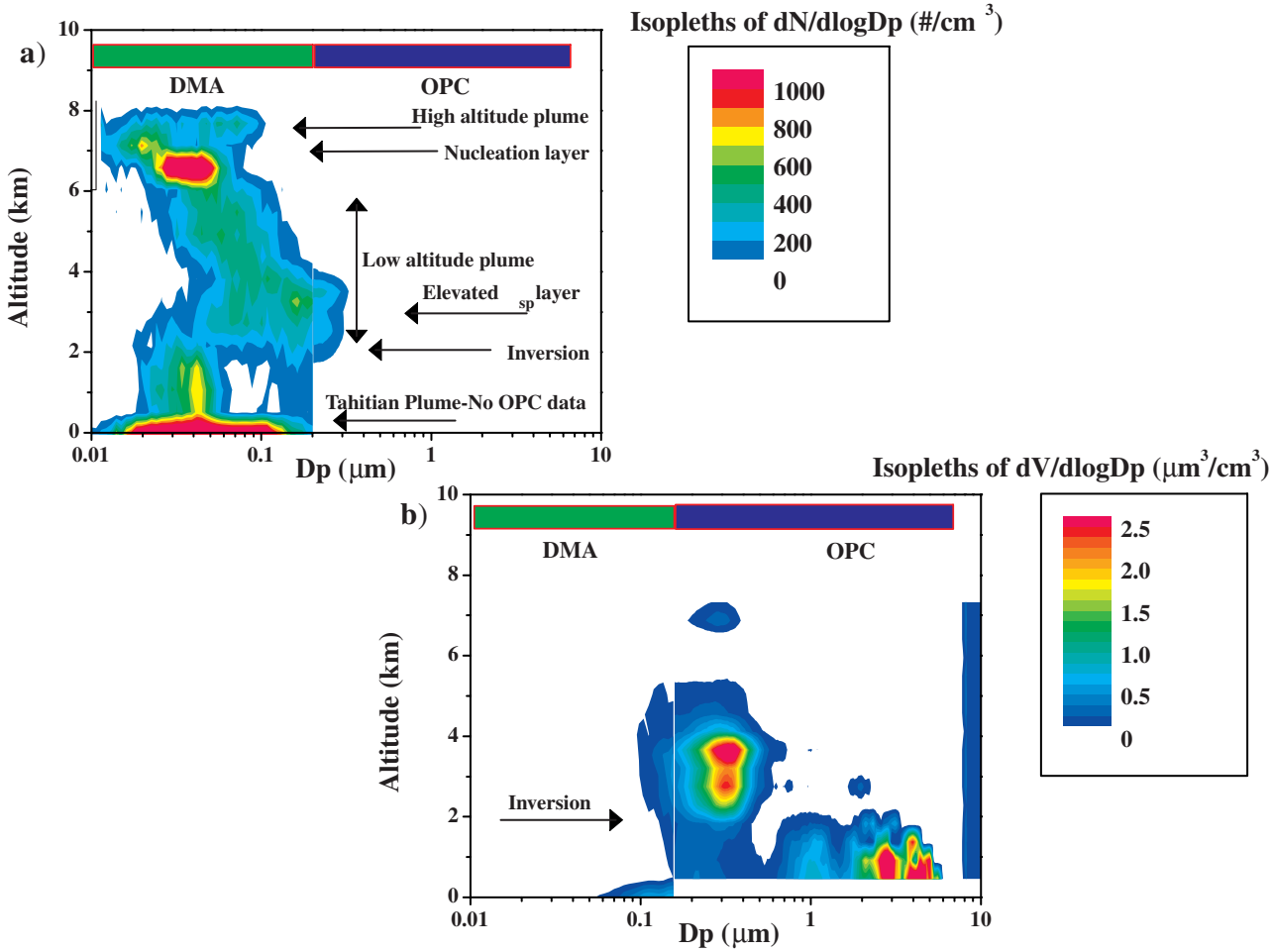

Figure 7. Same as Figure 2, but for region 3 (Central Pacific, PEMT A).

(Figure 9b). The coarse mode aerosol was mostly refractory (variation reflects low count statistics for the largest particles) as one expects for sea salt. The dry accumulation mode aerosol below 0.5 μm still contained most of its volume after heating to 150°C, consistent with a more neutralized aerosol constituent such as ammonium sulfate or bisulfate. The refractory volume left in this mode after heating to 300°C is associated with the leading edge of the sea salt distribution and not associated with combustion aerosol, as confirmed by the negligible light absorption measured for this case (less than 1×10^{-7} m^{-1}, Table 3).

[36] The number distributions for the FT (Figure 9c) were bimodal in nature. The predominant peak was located at approximately 0.025 μm, with a secondary peak at ~0.1 μm. There was little concentration remaining after heating the aerosol to 150 and 300°C, again consistent with a highly volatile aerosol (for both modes) in the FT. This volatile aerosol is most likely made up of sulfuric acid as is common in the "clean" marine FT, especially near the ITCZ where active nucleation and growth from sulfuric acid has been shown to occur regularly [*Clarke et al.*, 1999]. The MBL number distributions (Figure 9d) were bimodal as was discussed previously in regards to Figure 2a. The distribution for 150°C revealed a more neutralized aerosol than that found in the overlying FT. Since subsidence of aerosol from aloft has been identified as a primary source of MBL aerosol in this size range, this suggests the ammonia in the remote "clean" Pacific MBL is sourced at the ocean surface, consistent with results obtained by *Dibb et al.* [1999] and *Clarke and Porter* [1993].

3.3.2. Region 2: PEMT A Flight 18 (South American Outflow)

3.3.2.1. Vertical Structure

[37] Region 2 (Figure 1) is located west of South America and is primarily characterized by outflow from the continent. The profiles shown in Figures 4e and 4f (taken at the location labeled PR2 in Figure 1, approximately 78°W and 13°S) reveal a different vertical structure than that in the "clean" region. Elevated values of RCN ratio, scattering coefficient, and combustion gas phase indicators such as O_3 (Carrol, archive data) and CO (Sachse, archive data) are observed in the FT (especially between 2 and 6 km) and the aerosol and gas phase data exhibited similar structure. The average aerosol light absorption coefficient taken from horizontal legs within the FT plume was 3.8×10^{-6} m^{-1} (see Table 3). Elevated aerosol absorption coefficients indicate the presence of black carbon (BC), a combustion by-product and dominant aerosol absorber. Biomass indicators such as CH_3Cl [*Gregory et al.*, 1999] were elevated in this altitude range, consistent with a biomass-burning source for this plume. While the fairly uniform RCN ratio reflected similar aerosol character over this altitude range, the scat-

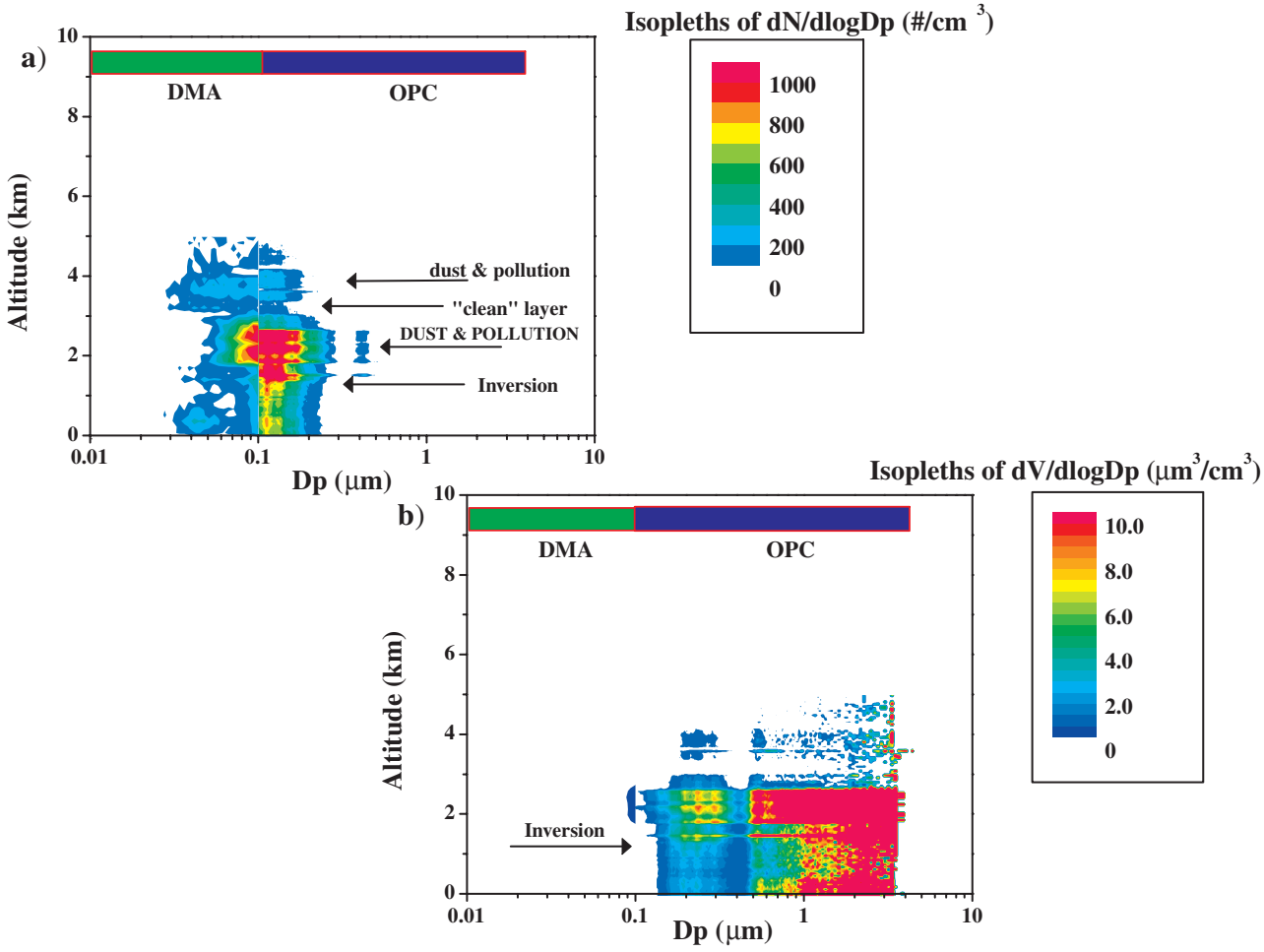

Figure 8. Same as Figure 2, but for region 4 (north Central Pacific, PEMT B).

tering coefficient exhibited several peaks, identifying layers of aerosol embedded within the larger FT plume. Since CN concentrations (Figure 4g) were relatively constant between 2 and 6 km, this layered structure in aerosol scattering should be due to variations in particle size. Between 1.75 and 2 km is a clearly identified "clean layer" where the combustion indicators were all low.

[38] UF concentrations are negligible throughout the bulk of the FT plume (2 to 6 km). However, there is a thin layer of UF located at 5.8 km where the RCN ratio has dropped below 0.25 and the RH (Figure 4h) is enhanced relative to the altitudes above and below it. This layer may represent prior nucleation from cloud outflow overlaying the background combustion plume. The aforementioned "clean layer" had much drier air associated with it (~5% RH) than the air above and below it while the bulk of the FT plume had relatively dry air (~25%). Clearly shown in the temperature profile (Figure 4h) was the presence of a strong inversion at approximately 1 km, which should have suppressed mixing between the FT and MBL.

[39] Below the inversion at ~1 km (within the MBL), there was some evidence for combustion influenced air. The scattering coefficient, gas phase indicators, and CN and RCN concentrations were considerably higher than in the "clean" MBL case (Figures 4a through 4c). Also, aerosol light absorption was elevated (2.48×10^{-6} m^{-1}) compared to the "clean" MBL, although not as high as in the FT plume above. It is possible that some pollution may have mixed down through the inversion. However, several gas phases more associated with urban/industrial emissions (SO_2 [*Thornton et al.*, 1999] and propane, for example) were elevated above background values, indicating a different source for the majority of the MBL plume (urban/industrial) than for the one located in the overlying FT (biomass burning).

[40] In the lower portion of the FT plume below 2.5 km and between the inversion (~1 km) and the "clean layer" (~2.0 km) there were intermediate concentrations of CO and O_3 (general combustion), CH_3Cl (biomass), and SO_2 and propane (urban/industrial indicators) than those found in the MBL and the overlying altitudes. Within these altitude ranges (1.0–1.8 km and 2.2–2.5 km), total scattering was significantly larger than subμm scattering, indicating the presence of coarse mode aerosol. Sodium concentrations from filter samples (Huebert, archive data)

Table 2. P3-B Vertical Profiles

Region	Latitude	Longitude	Experiment/Flight	Date
1	0°N	164°W	PEMT B/F12	26 March 1999
2	13°S	78°W	PEMT A/F18	22 September 1996
3	17°S	151°W	PEMT A/F12	5 September 1996
4	29°N	142°W	PEMT B/F18	10 April 1999

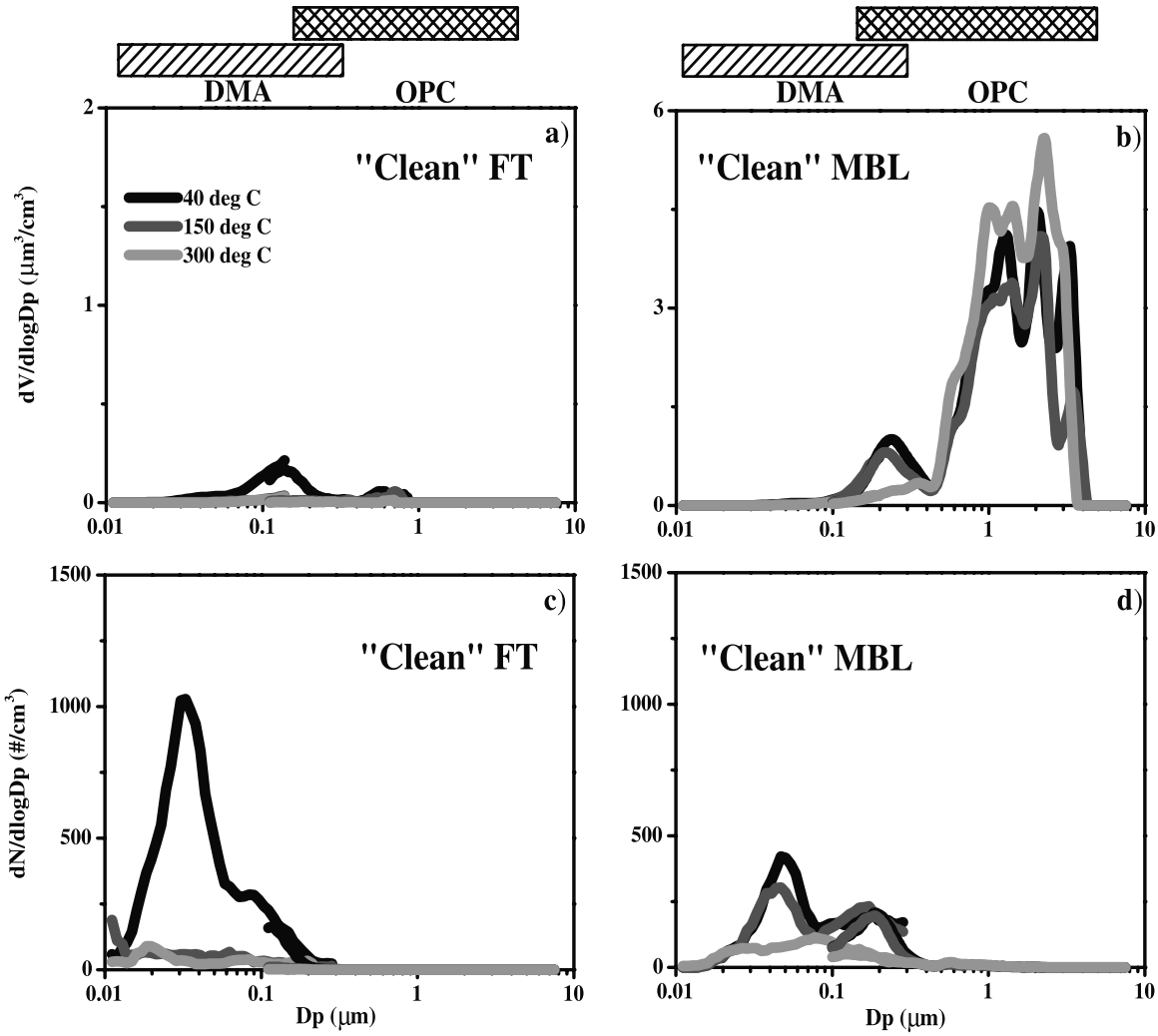

Figure 9. Aerosol size distributions and volatility at three temperatures for region 1. (a) shows the volume distributions for the "clean" FT (from ~4 km). Note the low volume and high volatility. (b) shows the volume distributions for the underlying MBL and exhibits the presence of significant refractory coarse mode aerosol (sea salt). (c) and (d) Number distributions for the "clean" FT and MBL, respectively.

collected on horizontal legs within these altitudes were enhanced when compared to the rest of the FT. These observations suggest that these levels contained a mixture of biomass burning constituents from above and urban/industrial combustion components and coarse mode sea salt from the underlying MBL. This mixing occurred despite the rather strong inversion evident in Figure 4h and an intervening "clean" layer at 2 km.

[41] Figure 6a shows the unheated number distributions (from both the RDMA and OPC) as a function of altitude. Above the inversion, the "clean" layer is clearly evident on the profile, as is the FT combustion plume above it. The peaks in scattering coefficient within the FT plume coincide with enhancements in larger particle sizes (Dp $\geq$ 0.2 μm) visible in the number distribution. Between the "clean" layer and the inversion, the unheated number distribution is very similar to those found in the overlying FT plume. The MBL number distributions exhibited the typical bimodal structure discussed previously for the "clean" region but there does appear to be a "connection" between the larger MBL mode and the size distribution immediately above the inversion, consistent with some of the aerosol from above mixing down into the MBL. Evidence that mixing had occurred between the biomass plume aloft and the MBL industrial plume is further illustrated in Figure 6b (unheated volume distribution profile). The levels centered at ~1.5 and ~2.5 km clearly show the presence of coarse mode aerosol.

[42] Some insight into the vertical structure of this region may be gained from the backtrajectories associated with the various altitudes. The FT plume (2–6 km), as already discussed, originated from the Amazon basin (a known biomass burning region at this time of year). The backtrajectory (not shown) for the "clean" layer (~2 km altitude) indicated that this air mass had traveled over the ocean from the northwest and had not passed over any continents in the previous 10 days. The MBL plume originated from the southeast, passing over Peruvian coastal cities just a few days prior to sampling. The differences in the backtrajectories (and in the gas phase indicators) are

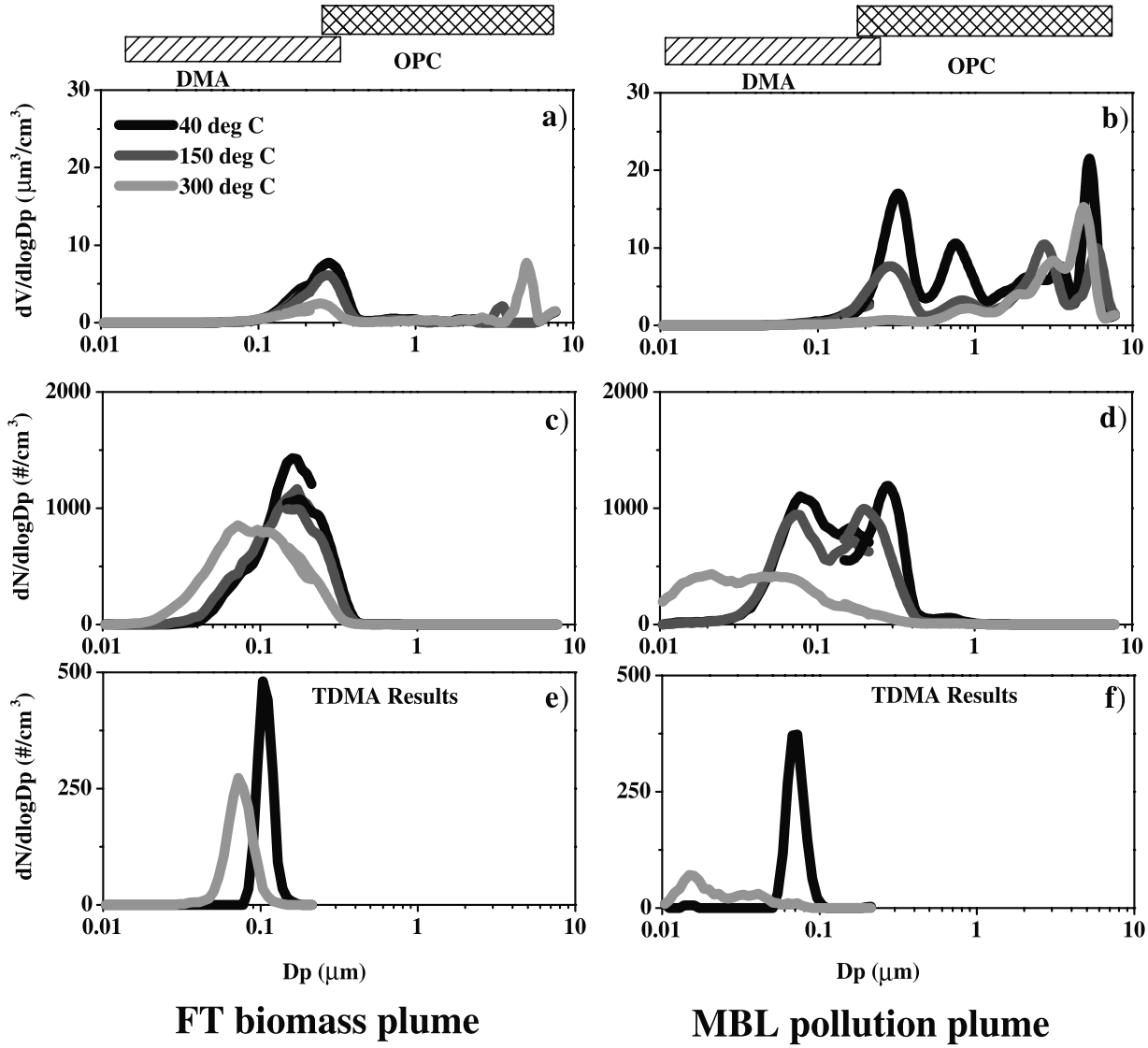

Figure 10. Same as Figure 9, but for region 2. (a) shows volume distribution for "mix" layer (~1.5 km) immediately above the MBL (pollution and some sea salt are present). Volume distributions for higher altitudes had the pollution component, but no large particles. (b) Volume distribution for MBL plume. (c) Number distribution for the FT pollution plume. (d) Number distribution for the MBL plume. (e) TDMA results for the FT plume. (f) TDMA results for the MBL plume.

consistent with the MBL and FT plumes having different sources, although there is some evidence of mixing of the two in the intermediate altitudes.

3.3.2.2. Size Distributions, Volatility, and TDMA Results

[43] The distributions for the MBL and FT plumes in the South American outflow region are shown in Figure 10. The volume distribution shown in Figure 10a was sampled at ~1.8 km altitude and shows a pronounced accumulation mode peak near 0.3 μm at all three temperatures. This includes a significant refractory component (remaining after heating to 300°C). Refractory coarse mode aerosols are also evident at this level. Volume distributions sampled at higher altitudes within the overlying FT plume had a very similar accumulation mode but with no coarse mode particles present. The refractory nature of this coarse aerosol, the proximity of this layer to the MBL, the enhancement in Na concentration (Huebert, archive data, see above), and the lack of coarse mode aerosol in the overlying FT all suggest that this aerosol was sea salt. The volume distribution sampled within the MBL plume (Figure 10b) was sampled at 500 m and shows a large sea salt component (refractory coarse mode aerosol) with a very significant accumulation mode aerosol present as well (peak at ~0.3 μm). In contrast to the volume distribution shown in Figure 10a, this accumulation mode aerosol was far less refractory. The refractory volume fraction (defined as the ratio of refractory to unheated accumulation mode volume) was 0.23 (23%) and 0.08 (8%) for the FT and MBL plumes, respectively, indicating a distinction in plume aerosol microphysics and chemistry that was also observed in the aerosol single scatter albedo (ω). The value of ω within the FT plume was 0.88 (Table 3) while within the MBL plume it was 0.98 (not shown). These correspond to ratios of aerosol light

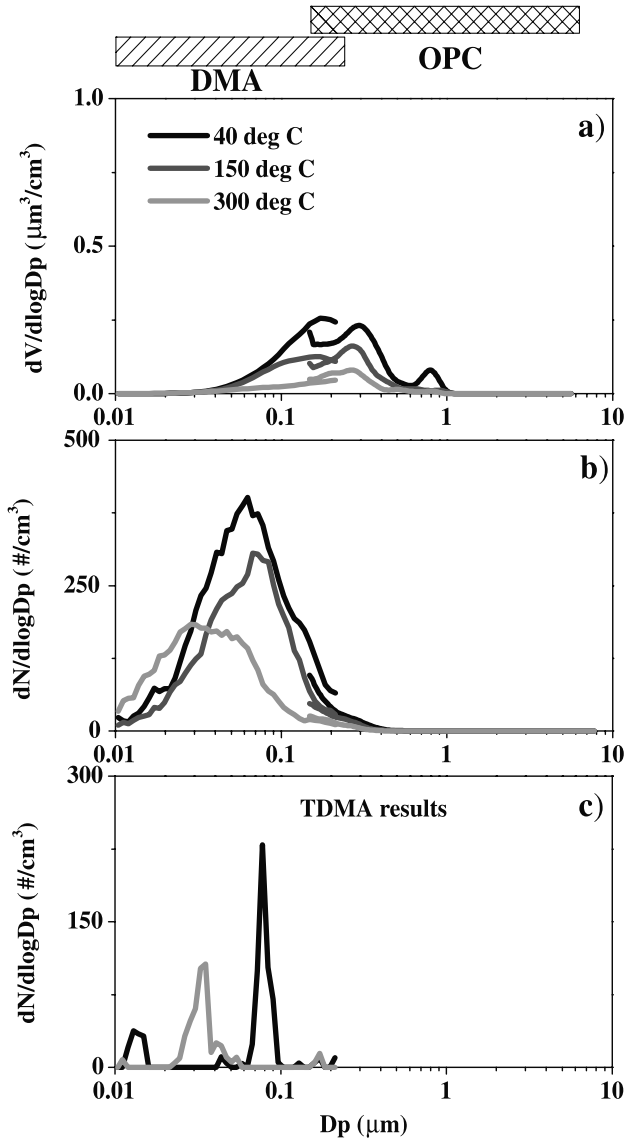

Figure 11. Same as Figure 9, but for region 3 plume taken at 4 km. Note the lack of coarse mode aerosol and the similarity of the TDMA results of this region to those shown for region 2 FT plume.

absorption to scattering coefficients of 13.6% and 2.0% for the FT and MBL plumes, respectively.

[44] These differences in aerosol size resolved physiochemistry are more pronounced when plotted as heated and unheated number distributions (Figures 10c and 10d, 1.8 km and 500 m, respectively). The 1.8 km distribution was monomodal and virtually unchanged after heating to 150°C, indicating neutralized sulfate aerosol; the refractory distribution (300°C) was also monomodal, but the peak diameter has shifted to smaller sizes. Within the MBL, the unheated number distributions are bimodal, consistent with cloud-processed aerosols [*Hoppel et al.*, 1986]. A comparison of the refractory number distributions shows that while the integral number of refractory aerosols is nearly equal in Figures 10c and 10d, the MBL refractory distribution was shifted to smaller sizes after heating compared to 1.8 km, suggesting different physical processes responsible for these two plumes and consistent with the previous discussion of the vertical structure within this region.

[45] Further demonstration of the differences in aerosol microphysics and chemistry is shown in Figures 10e and 10f (TDMA results for ~0.1 μm monodisperse sizes for the FT and MBL, respectively). The observed shifts in peak diameters after heating to 300°C are similar to the results obtained for the entire polydisperse distributions shown in Figures 10c and 10d and allow us to make qualitative statements as to the degree of internal versus external mixing of the aerosol constituents. The integral number remaining after heating was approximately conserved in the FT plume, showing that aerosol refractory components were generally well mixed internally with the more volatile aerosol. The FT plume showed a clearly defined and narrow peak after heating, indicating a uniform distribution of refractory components. While the MBL aerosols also appear to be internally mixed, the majority of the refractory aerosols are at much smaller diameters than those observed in the overlying FT. Also, there was a greater spread of the number distribution after heating in the MBL plume, indicating a variety of sized refractory aerosol associated with a given diameter in the unheated distribution.

3.3.3. Region 3: PEMT A Flight 12 (Central Pacific/ Long-Range Transport)

3.3.3.1. Vertical Structure

[46] The air mass characterized in region 3 (Figure 1) reflects subsiding westerly flow approaching the South Pacific Convergence Zone (SPCZ) from the southwest. Figures 4i through 4k contains vertical profiles of aerosol, gas phase, and meteorological measurements taken at the location labeled PR3 (approximately 151°W and 17°S) in Figure 1. There was a thick layer of enhanced RCN and RCN ratio and gas phase indicators from approximately 2 to 6 km and these variables tend to track each other reasonably well. The average aerosol light absorption within this plume was 2.8×10^{-7} m^{-1} (Table 3), again indicating BC and combustion influenced air. CH_3Cl concentrations (not shown) were also elevated above background values in this plume, suggesting a biomass-burning source [*Gregory et al.*, 1999]. Unlike the RCN ratio and gas phases, the scattering coefficient exhibited a marked difference between upper and lower portions of the FT plume (2 to 6 km); values are almost an order of magnitude greater in the lower 2 km than above it. This difference was not due to an increase in coarse mode aerosol since the submicron (not shown) and total scattering coefficients were nearly equal to each other at all altitudes above the MBL. There also appears to be a second layer containing enhancements of RCN ratio and combustion gases located at 8 km.

[47] Between 6 and 8 km, RCN concentrations decreased while CN and UF concentrations increased, suggesting "clean" air in this altitude range. A UF layer was observed at ~7.8 km just below the upper plume (8 km) in air with higher RH (~50%) and lower RCN ratio and may represent nucleation associated with the upper level plume mixing with "cleaner" air. The CN and UF concentrations (Figure 4k) were fairly uniform in the lower FT (altitudes <6 km). The combustion layers (2 to 6 km and 8 km) were present in

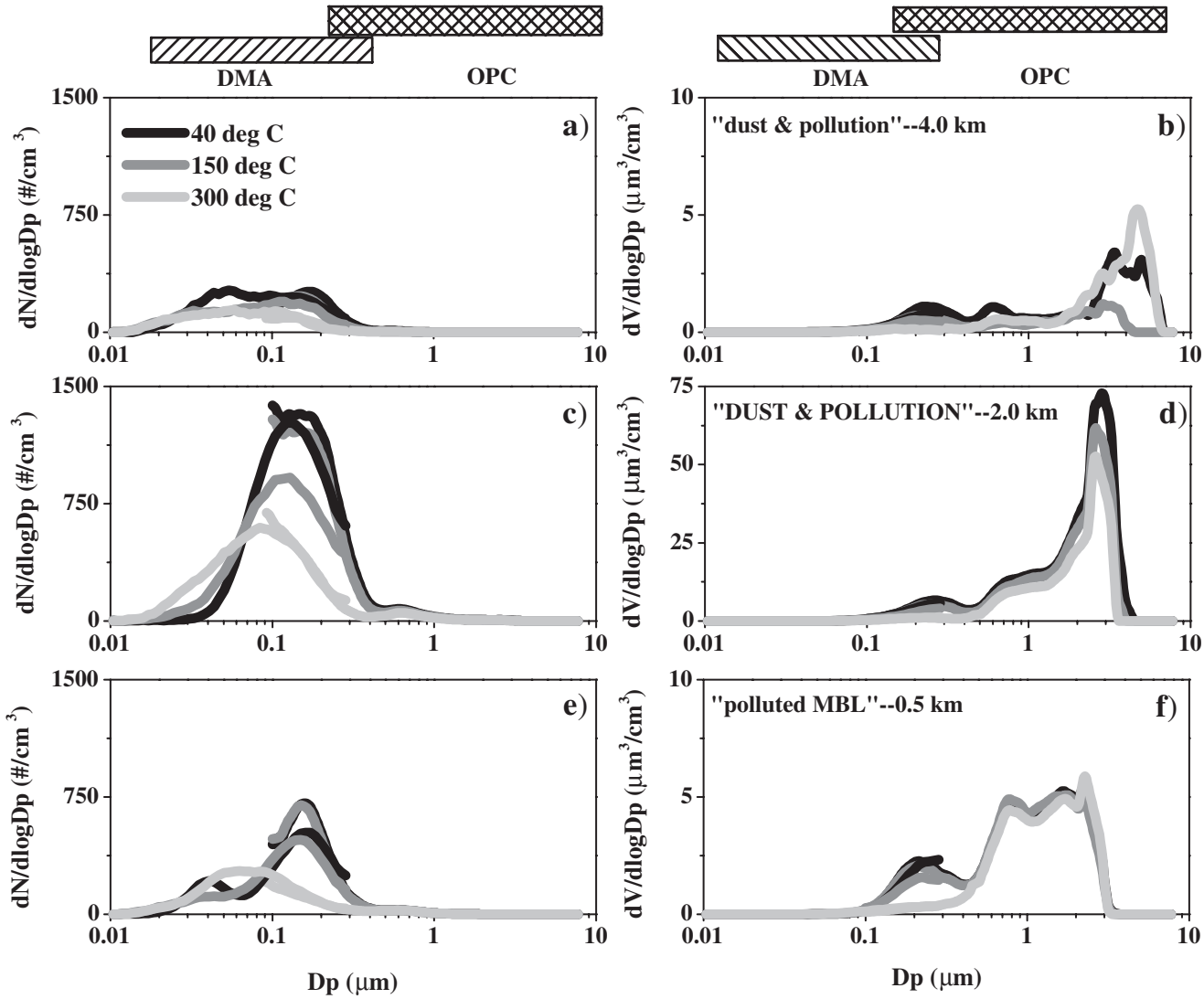

Figure 12. Same as Figure 9, but for region 4. (a) and (b) are data from 4 km altitude, (c) and (d) are from 2 km (corresponding to the layer with the highest coarse mode volume, note change in scales), and (e) and (f) are for the MBL. Note the presence of significant volume of coarse mode aerosol at all altitudes. Also note the similarity in the refractory aerosol shown in the number distributions at all three altitudes.

very dry air (RH < 25%, Figure 4l), similar to region 2. In contrast to region 2, the temperature profile (Figure 4l) showed no well-defined inversion separating the MBL from the FT (a weak inversion can be discerned at ~2 km).

[48] The low levels of RH, enhanced values of O_3, and increased potential vorticity in the primary FT plume (2–6 km) led some [*Stoller et al.*, 1999] to suggest that the air mass being sampled had a stratospheric component, or at least a "cap" of stratospheric air overlying the pollution plume. However, the amount of stratospheric air must be small since the plume contained an elevated RCN and RCN ratio and stratospheric aerosol (being far removed from surface sources of refractory components) are composed primarily of volatile sulfuric acid [*McCormick et al.*, 1993]. Also, this altitude range contained a significant concentration of CO, which is not associated with stratospheric air masses.

[49] The combined RDMA and LOPC unheated number distributions as a function of altitude are displayed in Figure 7a. The elevated scattering values between 2 and 3.5 km (Figure 4i) corresponded to an increase in concentration of larger accumulation mode particles (with $D_p \geq 0.15$ μm), but not to the presence of any coarse mode aerosol ($D_p \geq 1.0$ μm). The number distributions for particle diameters ≤0.1 μm were similar within the lower portions (2 to 3.5 km) and upper portions (3.5 to 6 km) of the primary FT plume. The higher concentration of larger accumulation mode aerosols with diameters greater than 0.15 μm (and corresponding increase in aerosol scattering) in the lower altitudes of the 2 to 6 km plume may be due to several reasons. Namely, the injection of the plume over the source region into higher altitudes would be more likely to remove the larger accumulation mode aerosol relative to injection into lower altitudes. The initial convective activity ("dry" and/or "wet" convection) responsible for this injection into the FT may have evolved over the course of a particular event (possibly reflecting the intensity of burning) or may

Table 3. Average Aerosol Properties of the "Clean" and Continental/Combustion Perturbed Regions Within the FT[a]

	Region 1 ("Clean") (Aged Marine Air)	Region 2 (South American Outflow)	Region 3 (Central Pacific Long-range Transport)	Region 4 (Asian Outflow)
		Microphysics		
Mean number Dp (μm) @40°C	0.03	0.19	0.08	0.16
@150°C	0.02	0.19	0.08	0.11
@300°C	0.01	0.09	0.025	0.08
Mean volume Dp (μm) @40°C	0.13	0.29	0.3	0.29
@150°C	0.12	0.28	0.29	0.28
@300°C	0.11	0.25	0.25	0.25
RCN ratio (refractory number fraction)	0.1	0.68	0.66	0.68
RVF (refractory volume fraction)	0.01	0.23	0.24	0.25
Mean submicron unheated integral volume, $\mu m^3/cm^3$	0.16	1.28	0.28	1.11
Mean submicron refractory integral volume, $\mu m^3/cm^3$	1.6×10^{-3}	0.29	0.06	0.28
		Optics		
σ_{sp} @550 nm (1/m)	2.98×10^{-7}	3.14×10^{-5}	2.13×10^{-6}	2.47×10^{-5} (9.90×10^{-6} for submicron component)
σ_{ap} @565 nm (1/m)	$\leq 1.00 \times 10^{-7}$	3.80×10^{-6}	2.80×10^{-7}	1.48×10^{-6}
"dry" ω (calculated from σ_{sp} and σ_{ap})	NA	0.89	0.88	0.94 (0.87 for submicron component)
"dry" ω (determined graphically)	NA	0.88	0.88	0.94 (0.86 for submicron component)
		Bulk Properties		
Experiment/flight	PEMT B/12	PEMT A/18	PEMT A/12	PEMT B/18
Location	Central Pacific (equatorial)	South American coast (equatorial)	Central Pacific (Southern Hemisphere tropics)	Northern Pacific (Northern Hemisphere midlatitudes)
Average RH, %	50	15	12	8
Altitude range of plume (and layers)	NA	2.2–5.5 km (2.2, 4.0, and 5.5)	2.2–4.9 km (3.0)	1.3–4.5 km (2.0 and 4.0)
Source region and type	"aged" marine air (NA)	South America (biomass)	Africa/Australia? (biomass)	Asia (industrial/urban and dust)
Source age	More than 10 days	5–10 days	More than 10 days	~10 days

[a] The altitude ranges presented in the table correspond to the bulk of the plumes (where the RCN ratio is above 0.5). In addition, the altitudes of layers within the plumes (as identified by elevated scattering coefficients and size distributions) are given in parenthesis. The average thickness of these layers was ~0.6 km.

have been episodic in nature with more rigorous vertical transport occurring during different phases of the convective activity. Also, after injection into the FT, additional aerosol may have been added from more ''localized sources'' to the lower portions of the preexisting plume. This subsequent addition of aerosol may have occurred immediately after the initial injection near the source region (presumably southern Africa) or downwind after long-range transport (Australia). It is also possible that the larger submicron particles found in the lower portions of the plume may have ''settled'' during long-range transport. Most models of long-range transport of aerosol plumes do not usually include the settling of submicron particles. However, this possibility is unlikely due to the small difference in ''settling velocities'' between particles with D_p = 0.1 and 0.2 μm (8.7×10^{-4} mm/s versus 2.3×10^{-3} mm/s, respectively, calculated from an in-house computer program using appropriate particle densities, etc.). Even after 10 days of transport (8.64×10^5 s), the difference in fall speeds would only lead to a separation of ~1 to 2 m for these size particles.

[50] Both the elevated UF layer (~7.8 km) and the high altitude plume (~8 km) are evident in the size distributions. Below the weak inversion near 2 km, the distributions above 500 m show the bimodal structure typically observed in the MBL, while the lowest 500 m is dominated by locally derived pollution emanating from Tahiti. The volume distributions (Figure 7b) show the coarse mode sea salt present within the MBL with little coarse mode volume aloft.

[51] The backtrajectories for the 2 to 4 km and 4 to 6 km (Figures 3a and 3d) altitude ranges in the primary FT plume in region 3 were similar. The most significant difference was that those arriving in the upper portions (4 to 6 km) of the primary FT plume extended back to Africa (after passing over Australia ~4 days before) within 10 days prior to sampling. Those at the lower altitudes (2 to 4 km) also passed over Australia and extended to the west toward the African coast. However, these backtrajectories did not reach Africa in the previous 10 days; they were over the Indian Ocean at that time. Unfortunately, the backtrajectories for these two altitude ranges do not explain the observed difference in scattering coefficients. The backtrajectories [*Fuelberg et al.*, 1999, Figure 18] for air parcels arriving at ~8 km when encountered by the aircraft originated from the northwest in the vicinity of the maritime continent (Indonesia-another biomass burning source region during this season) rather than Australia and/or Africa, and imply that this upper plume was not stratospheric in origin but did have a different source than the lower one.

3.3.3.2. Size Distributions, Volatility, and TDMA Results

[52] Figure 11 displays the size distributions and TDMA results from a 4 km horizontal leg within the primary FT plume (2 to 6 km). This level was just above the enhanced scattering layer located in the lower portions of the plume (2 to 3.5 km altitude) and should be considered to be more representative of the 4 to 6 km range.

[53] The volume distributions (Figure 11a) reveal some differences in the ''overlap'' region between the RDMA and LOPC (particularly for the unheated distribution). This can be understood since the two measurements and thermal sequences were not coincidental in time and there was variability of aerosol properties within the plume. The unheated volume distribution shows a peak at ~0.3 μm with peaks at slightly smaller diameters for the heated distributions (Table 3). These distributions are similar in shape, the degree of neutralization (from the difference in unheated and heated to 150°C), and the ratio of the refractory to unheated accumulation mode volume (~24% versus 23%) as in the previous region. The number distributions (Figure 11b) are also qualitatively similar to those in region 2, being monomodal and suggestive of an internally mixed aerosol. However, the peak diameter for each temperature was at smaller sizes and there was a lower concentration of aerosol with diameters greater than 0.1 μm. TDMA results are shown in Figure 11c and demonstrate that this FT plume was also internally mixed, but the peak size of the refractory aerosol was smaller for this region than in region 2.

[54] The biggest difference between the number and volume distributions in this region to the previous continentally influenced region (region 2) was the lower integral properties. The smaller integral volume (i.e., mass) is consistent with previous results [*Dibb et al.*, 1999; *Talbot et al.*, 1999] suggesting that the plumes sampled in this region of the PEMT A field campaign (central, tropical Pacific) have undergone scavenging at some point in the past (most probably in the convective event that initially injected the aerosol and gas phase constituents into the FT). Scavenging of aerosol mass would preferentially remove any coarse mode and the larger accumulation mode aerosol (with diameters greater than 0.1 μm) that may have been initially present. However, even after the presumed scavenging, the aerosol still maintains a continental signature.

3.3.4. Region 4: PEMT B Flight 18 (Northern Pacific/Long-Range Transport)

3.3.4.1. Vertical Structure

[55] In spite of the few flights on PEMT A and B in the northern hemisphere, plume events north of the equator were not uncommon. Region 4 is located to the northeast of Hawaii and the flow was dominated by subsiding anticyclonic flow around the subtropical high pressure system typically found in this region and season. Before encountering the high, the backtrajectories show rapid transport from Asia (Figure 3). Aerosol and gas phase parameters are shown in Figures 4m through 4p for the profile labeled PR4 (approximately 142°W and 29°N) in Figure 1. The RCN ratio was greater than 0.5 for all altitudes (including the MBL) and exhibited less structure than the previous profiles. Gas phase combustion indicators also were elevated throughout the profile. Like the previous combustion plumes, average aerosol light absorption was elevated (1.48×10^{-6} m^{-1}, Table 3) when compared to the ''clean'' FT, again indicating BC aerosol and combustion sources. However, there was little corresponding increase in biomass indicators such as CH_3Cl (Blake et al., archive data) and SO_2 levels were extremely high (Bandy et al., archive data). The inference is that this region was predominantly affected by urban/industrial emissions (at these altitudes), although some biomass-burning influences cannot be ruled out. In contrast to the RCN ratio and gases, the scattering coefficient and CN concentrations had a more complicated structure. There was a large difference observed between the submicron and total scattering for all altitudes, indicating the presence of significant quantities of coarse mode aerosol, even in the FT. The meteorological profiles (Figure 4p)

reveal extremely dry air (~10% RH) above the very strong temperature inversion. This inversion was even stronger than the one observed in region 2 and therefore should have been a more effective barrier to vertical mixing between the MBL and FT.

[56] The vertical structure shown in Figures 4m through 4p is also evident in the unheated combined LDMA and LOPC number distributions (Figure 8a). Compared to the previous continentally influenced regions, less dramatic diameter shifts in the profile of the aerosol size distributions were observed. The predominant difference between the various layers was in aerosol concentration. Below the inversion, the number distribution (Figure 8a) reveals a pronounced accumulation mode centered at 0.15 μm. In the lowest altitudes of the MBL (from the surface to ~500 m), a second smaller mode was also observed with a peak diameter at ~0.04 μm. The MBL accumulation mode in this region contained a higher concentration than the more bimodal MBL distributions observed elsewhere. The plate suggests that a significant fraction of the combustion aerosol in the FT is propagating into the MBL (note the apparent connection between the MBL accumulation mode and the FT combustion plume and the gradient in concentration).

[57] Previous number distribution profiles for regions 2 and 3 (Figures 6a and 8a, respectively) showed few coarse mode aerosols within the FT. However, this profile (Figure 8a) reveals the presence of substantial numbers of coarse mode particles, especially in the 1.5 to 2 km altitude range. These coarse mode aerosols were found above the inversion and in extremely dry air (RH ~ 10%), consistent with the presence of dust rather than sea salt. The backtrajectory for this region (Figures 4a and 4d) and modeling results [*Clarke et al.*, 2001] are also suggestive of coarse mode dust in the FT. The labeling in Figure 8a of the two layers as "DUST and POLLUTION" (~2 km) and "dust and pollution" (~4 km) reflects the relative amounts of the two constituents within the layers. The volume distributions (Figure 8b) show the lower layer contained more volume of both aerosol types (accumulation mode pollution and coarse mode dust) compared to the upper layer.

[58] The backtrajectory shown in Figures 4a and 4d for this region was for the air mass arriving in the lower (2 km) layer. One for the upper (4 km) layer [*Clarke et al.*, 2001, Figure 2] showed a similar history, passing over the Asian continent 5 to 10 days prior to sampling, traveling eastward over the Pacific basin before circulating around the subtropical high pressure system and subsiding to lower altitudes. While the air arriving between the two layers [*Clarke et al.*, 2001, Figure 2] in the "clean" layer (~3.5 km) labeled in Figure 8a also circulated around the subtropical high, it remained over the Pacific Ocean during the previous 10 days and therefore did not acquire a continental signature.

3.3.4.2. Size Distributions and Volatility

[59] The number and volume distributions shown in Figure 12 for region 4 were taken at 3 levels within the profile corresponding to the labels "MBL" (0.5 km), "DUST and POLLUTION" (2 km), and "dust and pollution" (4 km) in Figure 8. Significant coarse mode volume was observed at all three temperatures, particularly for the distribution corresponding to the level labeled "DUST and POLLUTION" (note the change of scales). The refractory nature of this coarse aerosol, the associated backtrajectory discussed previously, and the extremely low value of RH (~10%) found above the inversion are consistent with the interpretation of the aerosol as dust (within the FT). The majority of the coarse mode aerosol in the MBL is likely to include sea salt, but the downward mixing of aerosol suggested in Figure 8a is consistent with pollution and dust components being present.

[60] The unheated accumulation mode aerosol in all three levels had a volume peak diameter of ~0.28 μm (similar to the other FT plumes discussed previously) and at smaller diameters in the heated distributions (Table 3). The presence of a refractory component in the accumulation mode, elevated absorption coefficients (1.48×10^{-6} m^{-1}), and high concentrations of ozone and CO (Figure 4n) justify its labeling as combustion/continental aerosol. The degree of neutralization (difference between unheated and heated to 150°C) and the relative fraction of refractory aerosol (refractory volume fraction ~25%) appears quite similar to the accumulation mode aerosol found within the other FT plumes and suggests that the submicron component of the optical properties should exhibit similarities to those of the other combustion/continental plumes. Due to the significant coarse mode dust, it would not be expected that the total (submicron plus coarse mode components) optical properties would be the same.

[61] The number distributions at all three levels suggest that the refractory aerosol component is relatively well mixed internally with volatile aerosol components, consistent with the other combustion/continental plumes found in the FT. The distributions from the "dust & pollution" level (Figure 12a) appear to be broader and less concentrated than the distribution from the lower level (Figure 12c), hinting at differences in aerosol microphysics. However, the most optically active portion of the size distribution (the accumulation mode) appears to be similar (see the corresponding volume distributions in Figures 12b and 12d). The MBL number distribution (Figure 12e) shows the bimodal structure typically observed in the MBL. However, in contrast to the other regions discussed, the concentration of particles with diameters ≥0.1 μm was enhanced compared to the concentration of particles in the smaller diameter mode. The refractory number distribution for this level was similar to that in the overlying FT (in contrast to the discussion of the MBL plume observed in region 2). Generally speaking, the MBL number distributions (Figure 12e) suggest that FT pollution was mixing into the MBL despite the very strong inversion displayed in Figure 4p.

4. Discussion

[62] Continental plumes in the FT were identified in the remote Pacific atmosphere by enhancements in gas phase/aerosol data and were found to seriously perturb characteristics of the "pristine" marine atmosphere. A summary of various aerosol and bulk properties of these plumes (within the FT) is contained in Table 3. Representative values of the various parameters from the "clean" FT are included to gauge the magnitude of these perturbations from the natural, background conditions. Particle light absorption data was within the instrumental noise ($\sim 1 \times 10^{-7}$ 1/m) and therefore it and ω were not reported for the "clean" FT case. Here we have identified FT plumes by requiring them to

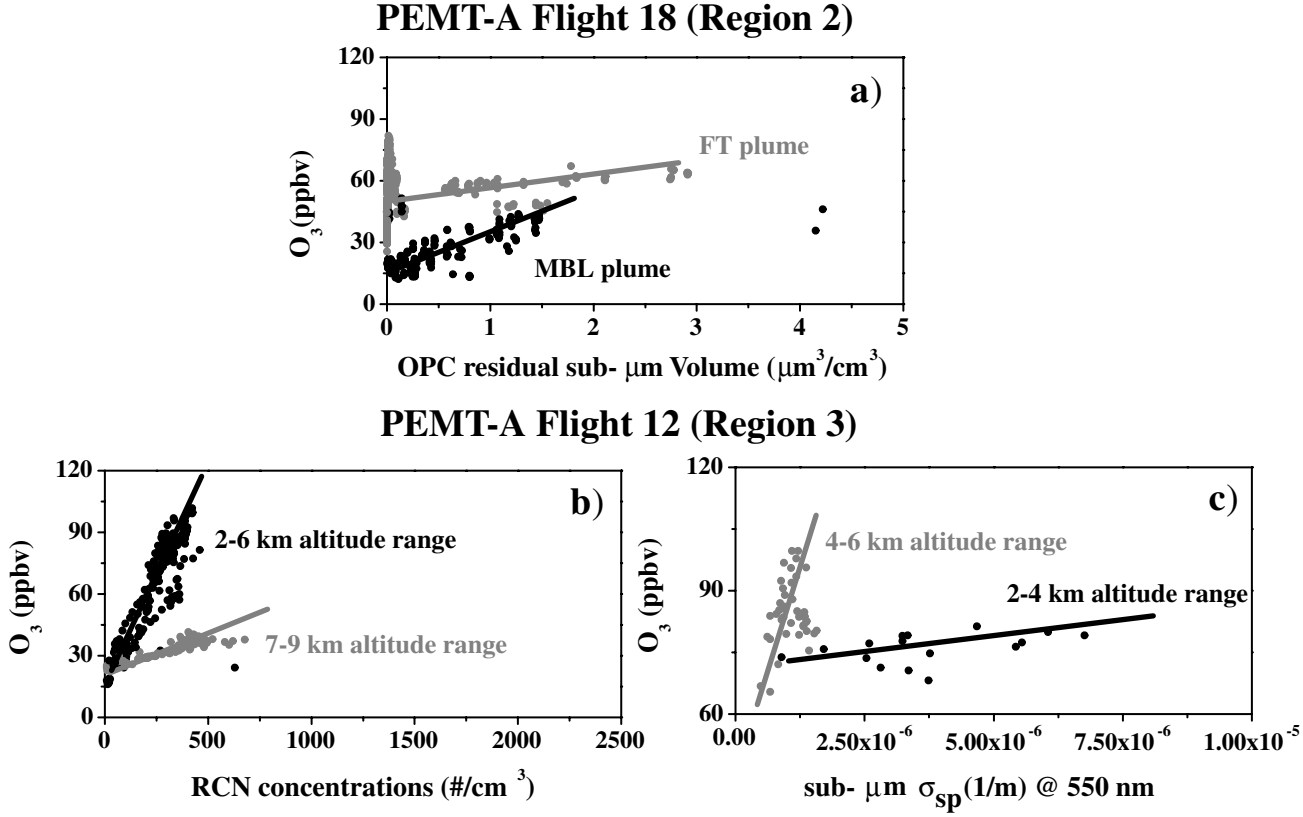

Figure 13. Scatterplots of ozone and various aerosol combustion indicators in plumes located in all three regions. (a) Region 2, refractory submicron volume versus ozone. (b) Region 3, RCN concentration versus ozone. (c) Region 3, submicron scattering versus ozone.

have a RCN ratio of 0.5 or greater (see Figure 4). The data for the "clean" FT and the FT plumes was for altitudes above 2 km (selected as the average height of the inversion separating the FT from the MBL). Source regions and types were inferred from chemical tracers (gas phase indicators) and backtrajectories. The "ages" for the various air masses listed were roughly estimated from the backtrajectories (time since passing over possible sources) and photochemistry (ratio of NMHCs to CO [*Gregory et al.*, 1999]). All three regions had aerosol characteristics much different than in the "clean" case. Notably, the light scattering and absorption coefficients in the "younger" FT plumes (regions 2 and 4, South American and Asian outflow, respectively) were similar to reported urban/industrial values [*Waggoner et al.*, 1981] and approximately two orders of magnitude higher than in the "clean" region. This is reflected in some of the aerosol size distribution characteristics as well. In particular, the peaks of the number distribution (at all three temperatures) were at larger values of D_p and the integral volumes were higher than in the "clean" region. The "older" plume (region 3, Central Pacific long-range transport) exhibited intermediate values of these parameters (integral volume and light scattering and absorption coefficients, Table 3). As previously discussed, other researchers [*Dibb et al.*, 1999; *Talbot et al.*, 1999] reported observations suggestive of extensive scavenging for the continental FT plumes sampled in this region of the PEMT A field campaign. One would expect lower integral properties (volumes, optical properties, etc.) for scavenged plumes. However, other more intensive properties (such as RCN ratio, refractory volume ratio, and submicron ω) might still be expected to maintain their continental signature, and in fact these values are similar for all the FT plumes.

[63] Peak volume diameters (at all three temperatures) were similar and the accumulation mode refractory volume fraction was ~0.24 in all three regions. Also, the RCN ratio was fairly consistent at ~0.67, reflecting the internally mixed character of the aerosol. Region 4 (Asian outflow) had a higher value of ω than regions 2 and 3 due to the presence of significant coarse mode aerosol (dust). Dust is a much more efficient scatterer than absorber and will raise the single scatter albedo. However, as will be discussed below, the submicron component of ω (excluding the coarse mode dust and more relatable to the combustion component) is very nearly the same for all three regions. The average RH values within these plumes were consistently lower than 40% (see Table 3) and therefore there would be little correction for RH affects (i.e., hygroscopic growth) for their associated optical properties and size distributions.

4.1. Gas Phase and Aerosol Relationships in Continental Plumes

[64] The data above demonstrate the presence of extensive plumes of continental outflow extending over large portions of the Pacific basin with enhanced aerosol and gas

phase combustion indicators. Vertical profiles often suggested trending between the gas phase and aerosol properties. Figure 13 displays scatterplots between some of aerosol combustion indicators and O_3 concentrations.

[65] The data presented for region 2 (South American outflow) suggested the presence of two plumes; a biomass plume located in the FT and a MBL plume described as influenced by urban/industrial sources from the South American coast. O_3 concentration is plotted as a function of refractory accumulation mode volume in Figure 13a. This aerosol combustion parameter exhibits a linear relationship with ozone. When separated by altitude, a different relationship (slope) is seen between the MBL and FT plumes, further supporting the earlier assertion that the two plumes are distinct and have been generated by different sources.

[66] While different processes act on O_3 and aerosols in the FT and MBL (e.g., cloud processes) and might change the observed relationship shown in Figure 13a, the backtrajectories suggest that this difference is related to sources and not processes. Combustion from urban/industrial sources (i.e., the MBL plume) is likely to be more efficient than from biomass burning (i.e., the FT plume) and one might expect that the relationship of ozone to the resulting mass of soot (i.e., refractory accumulation mode volume) would be different in biomass burning (different slope).

[67] Other aerosol combustion indicators should also exhibit relationships with the various combustion gases. In Figure 13b, RCN concentration is plotted versus ozone for region 3 and a linear relationship is evident. However, it is clear from the figure that there are two branches on the plot. After sorting by altitude, the lower branch corresponds to the previously identified plume at ~8 km altitude while the upper branch represented the lower FT biomass plume (2 to 6 km). This supports the previous assertion that these two plumes were distinct and that they were emitted by different sources (Indonesia versus Australia/Africa).

[68] Aerosol optical properties (submicron and total scattering coefficients for example) showed enhancement within the various plumes and could be expected to display a positive relationship with other combustion indicators. Submicron σ_{sp} is plotted versus ozone in Figure 13c and does indeed reveal that these two parameters are linearly related in region 3. Aerosol optical properties have typically been the most accessible to remote sensing techniques (including Lidar and satellite measurements) and any links between these properties and gas phase concentrations could prove useful for interpreting remotely sensed data in the future.

[69] In discussing the vertical structure found in region 3 (Central Pacific long-range transport), it was pointed out that the optical properties in the plume are approximately an order of magnitude greater in the 2–4 km than in 4–6 km range (see Figure 4i). This distinction is clearly defined in Figure 13c and shows a very different relationship between submicron σ_{sp} (more closely related to the combustion component) and ozone for the two altitude ranges. The higher values of ozone concentration for a given scattering coefficient may indicate a stratospheric component in the upper levels of this plume, consistent with *Stoller et al.* [1999]. However, the RCN/ozone relationship (Figure 13b) and the aerosol and gas phase observations from this region are consistent with a single biomass plume in the 2 to 6 km range. The branching seen in the Figure 13c would then represent differences in processing (scavenging, etc.) and mixing of the plume as it traveled to the sample location.

4.2. Mixing and Nucleation at Plume Boundaries

[70] Mixing of these plumes with "clean" air could alter any relationships between aerosol and gas phase measurements. Also, plume boundaries (where plumes with high concentrations of precursor gases but substantial preexisting aerosol surface area and lower RH are mixing with "clean" air with higher values of RH and lower surface area) might provide ideal conditions for the formation of new particles (i.e., nucleation). The location of the profiles, backtrajectories, and size distributions discussed previously were chosen to illustrate characteristics in the "heart" of the plumes and not their edges. Opportunities to explore plume boundaries occurred on other flights.

[71] PEMT A flight 13 was the transit flight from Tahiti (region 3) to Easter Island (a "clean" region). The time series (Figure 14a) of RCN ratio, altitude, and UF concentrations show the transition from plume (high RCN ratio, low UF) to "clean" air (low RCN ratio, high UF). After crossing the abrupt plume boundary, UF concentrations increased (suggesting recent nucleation). RCN concentrations are positively related with O_3 within the plume (Figure 14b) as was the case for all three of the regions discussed previously. Unlike the other cases, however, unheated CN are negatively related with ozone (Figure 14c). This is what one may expect for mixing of plumes (high RCN and ozone concentrations) with "clean" air aloft (lower RCN/ozone and frequently higher volatile CN concentrations). This is because both ozone and RCN were associated with combustion in the source region while unheated CN were more closely associated to the natural formation process in clean air. Hence, RCN are a preferred tracer for combustion aerosol in the FT as opposed to total (unheated) CN.

[72] Size distributions within the plume boundary (not shown) for this flight revealed two distinct modes. One mode (with high concentrations and at smaller sizes) is highly volatile while the other mode (lower concentrations and at larger sizes) is more refractory and as such is more representative of the combustion aerosol. The more volatile mode is more associated with "clean" air and these two modes are externally mixed. Nearer sources both CN and RCN tend to correlate with ozone, reflecting the internally mixed character discussed earlier.

4.3. Aerosol Microphysics and Optical Properties in Plumes

[73] The aerosol number and volume distributions measured within the various plumes provided insights into the nature of the aerosol, degree of internal versus external mixing, scavenging of aerosol mass, and plume sources. Volume distributions were also informative as to the presence of any coarse mode aerosol (sea salt and/or dust). Intensive aerosol properties (integral number, volume, scattering coefficient, etc.) did vary for the three regions (see Table 3). Despite these differences, the volume distributions consistently revealed some similarities among the various

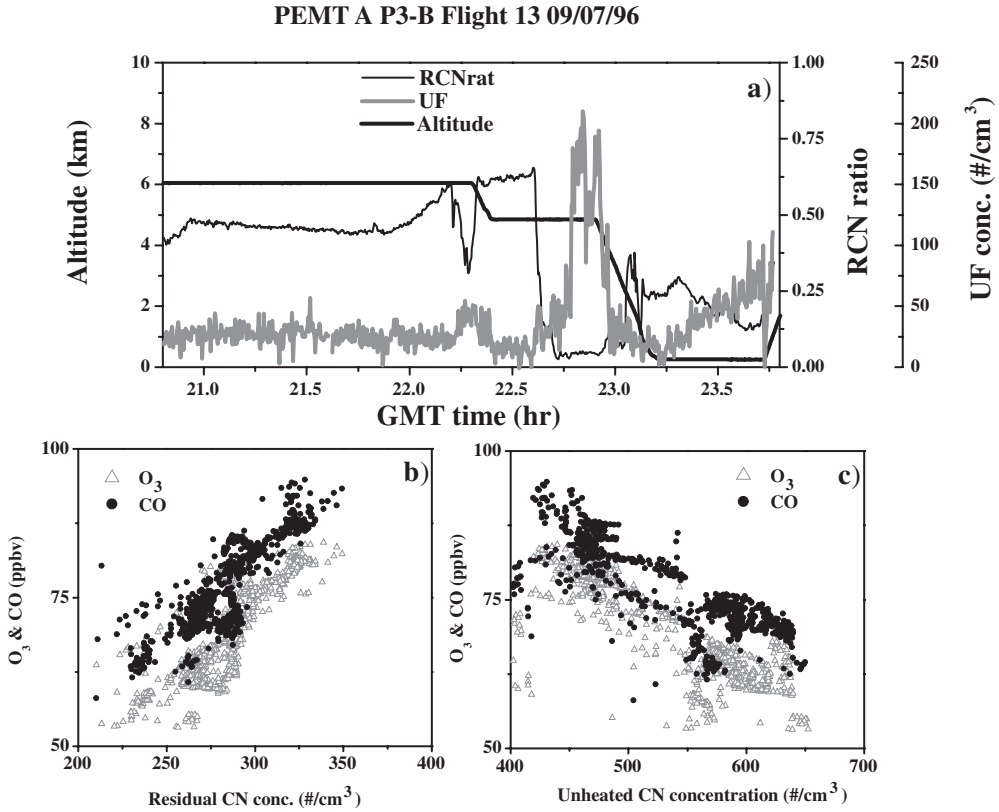

Figure 14. Evidence for mixing at plume boundaries. (a) Time series of RCN ratio, UF concentration, and altitude for PEMT A flight 13 (ferry flight from polluted region 3 to a ''clean'' region near Easter Island). (b) Scatterplot of RCN to ozone and CO (positively related) within plume. (c) Scatterplot of unheated CN to ozone and CO (negatively related) within plume.

continental plumes (particularly when encountered in the FT). Most notably, the peak diameters (at all three temperatures) were consistent at ~0.3 μm and the relative proportions of the integral volumes at the three temperatures were relatively uniform (the accumulation mode refractory volume fraction was about 25% for all plumes).

[74] These similarities and differences in aerosol microphysics/chemistry should be reflected in the aerosol optical properties for the various FT continental plumes. Figure 15 plots relationships within the plumes among several of these aerosol properties (averaged over horizontal legs within the FT and having an RCN ratio $\geq$0.5) for all three regions. Since the aerosol optical properties were not corrected to STP conditions, non-STP corrected integral accumulation mode volumes (unheated and refractory) were used in this figure. This would not effect the following conclusions since we are utilizing ratios (slopes) where the STP correction terms would cancel. Shown in Figure 15a is the linear relationship between the absorption and scattering coefficients. For the FT plumes encountered in regions 2 and 3, the total and submicron σ_{sp} were nearly identical (for most altitudes) and allowed for the use of total scattering coefficients in the figure. For PEMT A data (regions 2 and 3), the regression line (black solid line) had a R^2 value of 0.84. The continental emissions encountered in region 4 contained coarse mode dust (which should skew the relationship of total scattering to absorption). Therefore, Figure 15a contains the relationship of absorption to both total and submicron σ_{sp} for this region and the inclusion of dust aerosol has shifted the total scattering to larger values for a given value of absorption. For the PEMT B (region 4) relationship of total scattering to absorption (dashed gray line), the R^2 value was 0.93. For the region 4 relationship of submicron scattering to absorption (solid gray line), the R^2 value was 0.96.

[75] The radiatively important single scatter albedo (ω) for the various plumes can be determined from the slope of the regression lines (neglecting the small y-intercepts) relating absorption to scattering ($\omega = 1/(1 + \text{slope})$). Despite the differences in the biomass FT plumes sampled in regions 2 and 3, values of ω obtained by this method were very similar (~0.88). Also, the graphically determined values of ω were close to values calculated directly from the average scatter and absorption coefficients (see Table 3). The values of ω obtained for the plumes containing significant quantities of coarse mode aerosol were much higher at ~0.94 and ~0.98 for the region 4 FT plume and region 2 MBL plume (not shown), respectively. Figure 15a also shows the relationship of submicron scattering to absorption for region 4 and the value of ω obtained for the submicron aerosol component is very similar (~0.86) to the values determined for regions 2 and 3 FT plumes. The region 3 FT plume contained some coarse mode aerosol, but only in the lowest altitudes. This behavior indicates that the submicron soot dominates the majority of absorption in dust/pollution plumes; coarse mode dust has a small contribution to

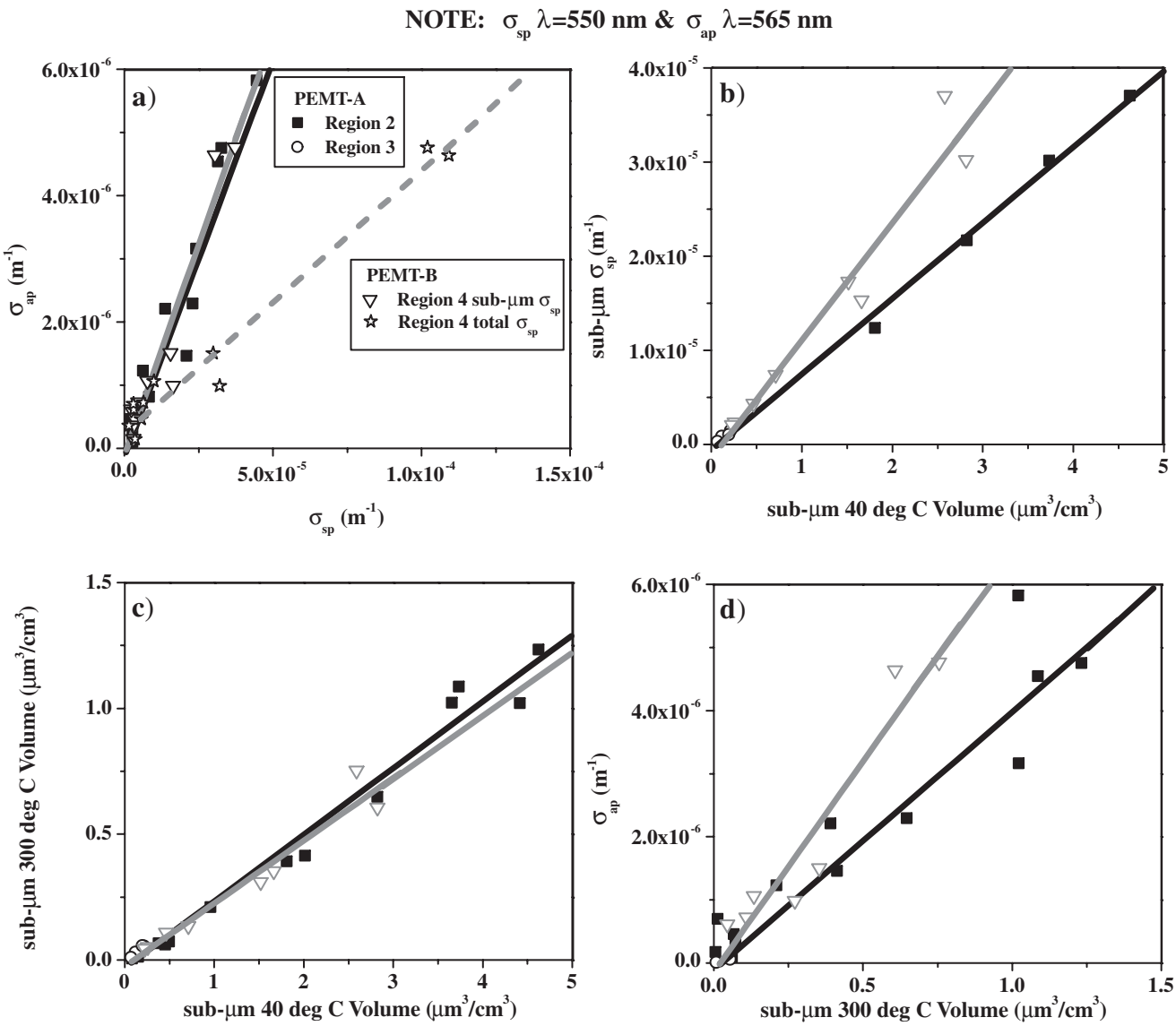

Figure 15. Scatterplots for horizontal leg averages of aerosol optical and volume measurements for regions 2, 3, and 4 within the FT. (a) Relationship of measured absorption coefficient to both total and submicron scattering coefficients. (b) Relationship of refractory to unheated accumulation mode volume. (c) Relationship of submicron scattering coefficient to unheated accumulation mode volume. (d) Relationship of absorption coefficient to refractory accumulation mode volume. The range of diameters for the accumulation mode volumes are from diam $\leq$1.0 μm. In (a), the black solid regression line is for PEMT A, the gray solid line is for PEMT B submicron data, and the gray dashed line is for PEMT B total data. In the remaining figures, the black solid regression line is for PEMT A, and the gray solid line is for PEMT B data. R2 values for each of the lines are reported in the text.

absorption, a large contribution to total scattering, and higher resulting single scatter albedos. In other words, the coarse mode dust will not greatly affect the absorption of the soot/dust mixture but will significantly increase the total scattering, resulting in higher ω values. When one uses just the submicron scattering relationship to the absorption, derived values of ω are similar to plumes that contained little or no dust.

[76] Plumes with very different sources and distances from these sources still exhibit a similar value of ω (for the submicron component) within the FT. This similarity might reflect some common behavior in aerosol microphysics for combustion plumes undergoing convective injection into the FT and subsequent long-range transport. As was stated previously, all of these plumes have a nearly identical accumulation mode refractory volume fraction of approximately 25% (see Figure 15c). R^2 values were 0.98 for PEMT A regions 2 and 3 data and 0.94 for PEMT B region 4 data (black solid line and gray solid line, respectively). If the accumulation mode refractory volume is at least partially composed of soot, the refractory volume should be correlated with absorption (Figure 15d). R^2

values were 0.85 for PEMT A regions 2 and 3 data and 0.92 for PEMT B region 4 data (black solid line and gray solid line, respectively). Similarly, unheated accumulation mode volume should be correlated with submicron scattering (Figure 15b). R^2 values were 0.99 for PEMT A regions 2 and 3 data and 0.94 for PEMT B region 4 data (black solid line and gray solid line, respectively). Therefore, similarities in the ratio of these two volumes (Figure 15c) should be reflected in the ratio of absorption to scattering, resulting in similar ω values.

[77] The positive linear relationship between accumulation mode refractory volume and absorption (Figure 15d) supports the assertion that at least a significant component of this volume is BC. However, if the refractory volume were entirely BC, the slope of this relationship would be different. The specific absorption of BC aerosol depends on a number of factors, including the size distribution [*Clarke et al.*, 1987], and reported values range from 5 to 15 m^2/g [*Liousse et al.*, 1993]. The peak diameter of the refractory distribution was nearly 0.25 in all plumes; therefore an appropriate specific absorption of 8.5 m^2/g [*Clarke et al.*, 1987] was selected. Using this value and a density of 2.26 g/cm^3, the resulting slope of the regression line between refractory volume and absorption would be 1.9×10^{-5} $(1/m)(cm^3/\mu m^3)$. The slope is 4.2×10^{-6} $(1/m)(cm^3/\mu m^3)$, suggesting that only 22% of this refractory volume (and therefore only ~5.5% of the total unheated volume) is BC (the predominant absorbing aerosol [*Heintzenberg*, 1982]) and that other refractory components were present. These include fly ash, nonvolatile organics (NVOs), and other refractory carbonaceous aerosols. Recent experiments (INDOEX) [*Ramanathan et al.*, 2001; ACE-ASIA, B. Heubert, personal communication] have shown that the mass of organic carbon (OC) is often as large (or even larger) as any other aerosol component (including sulfates) within combustion plumes sampled in the FT.

[78] The data for all three regions showed lower values of ω in the FT than in the underlying MBL, even when the MBL was polluted. The tendency for lower and less variable "dry" ω values aloft suggest that surface measurements may tend to overestimate ω (underestimate relative absorption) for the atmospheric column. This is important since most aerosol data from the remote Pacific Ocean are surface based.

5. Conclusions

[79] The RCN ratio was useful in identifying combustion/continental plumes and showed trending with the combustion gases. We have examined 3 regions that had substantial influence from continental sources. PEMT A was mostly influenced by biomass burning in austral spring (Southern Hemisphere tropics, regions 2 and 3) and PEMT B showed long-range transport of urban/industrial plumes with Asian dust in spring (Northern Hemisphere midlatitudes, region 4). The horizontal scales of these FT plumes were hundreds to thousands of kilometers and the distance of transport varied from ~1500 km (near the South American coast, region 2) to over 10,000 km (for plumes located in the central Pacific-regions 3 and 4). The bulk of these plumes were found to be located in the free troposphere (FT) in the 2 to 6 km altitude range (see Table 3), with most of the aerosol mass (as inferred from enhanced integral volume and scattering coefficient) typically being confined to the lower 2 km of the plumes (2 to 4 km altitude).

[80] The vertical profiles of these plumes showed the vertical extent, layering, and evidence of vertical mixing (despite the strong temperature inversions observed for two of the four regions). The complex layering of some aerosol properties (size distributions and scattering coefficients, for example) revealed structuring within the larger scale plumes that was not readily identified in other plume indicators (CN/RCN concentrations, RCN ratio, and gas phase data) despite the rather large vertical excursions of these plumes evident in the backtrajectories. The vertical extent of theses plumes (identified by RCN ratio >0.5) was typically 3–4 km (see Table 3). The vertical range was from just above the inversion between the MBL and FT (~1.5–2 km altitude) to 6 km altitude. The layers within the larger scale plumes were typically 0.6 km thick and layer altitudes (identified from elevated aerosol scattering coefficients) are given in Table 3. This structuring should be included in any model used to estimate the "direct" radiative forcing of these plumes (i.e., these plumes are not homogeneous "blobs" extending throughout the FT). It should be noted that regions 2 (South American outflow) and 4 (Asian outflow) were located over extensive stratocumulus cloud decks and the presence of these low level, high albedo clouds will increase the "direct" effect on radiative forcing [*Heintzenberg et al.*, 1997]. The subsidence of this combustion aerosol into the MBL can be expected to affect "indirect" forcing (through the enhancement in particles with diameters $\geq$0.1 μm and resulting perturbation on CCN number spectra [*Twomey et al.*, 1984]) and the hydrological cycle (through the suppression of precipitation [*Rosenfeld* 1999]).

[81] During PEMT A and B, most continental/combustion plumes were encountered in relatively dry air. This allowed us to neglect hygroscopic growth corrections to the size distributions and optical properties (see discussion of RH effects in the instrument section). Field campaigns in other regions (especially those relatively close to the source region) revealed emissions under a variety of RH conditions (dry, wet, and intermediate). However, those that sampled in more remote locations (implying long-range transport) frequently encountered plumes within dry, subsiding, stable air, including ASTEX [*Clarke et al.*, 1997] and TRACE-A [*Fuelberg et al.*, 1996]. Stable layers within the FT would be expected to limit vertical mixing, thereby diminishing dilution of any plumes contained therein. Also, plumes that were lifted to the mid to upper FT would encounter higher average wind speeds (and lower RH) that would facilitate their transport to greater distances from their respective source regions.

[82] Size distributions and associated volatility revealed differences in aerosol microphysics/chemistry for the various plumes, especially in integral properties (total number, volume, etc.). Similarities were also observed, including the peak diameter of ~0.3 μm for the unheated accumulation mode volume distribution and most plumes were without coarse mode aerosol. However, region 4 (Asian outflow) contained significant volumes of dust and the presence of this coarse mode aerosol affected the observed aerosol optical properties. The unheated accumulation mode volume

peak diameter was similar to reported values for other experiments, including TARFOX [*Hartley et al.*, 2000; *Remer et al.*, 1999], SCAR-B [*Ross et al.*, 1998; *Reid and Hobbs*, 1998], ASTEX [*Clarke et al.*, 1997], TRACE A [*Anderson et al.*, 1996a], and SAFARI-92 [*Le Canut et al.*, 1996]. The "clean" FT aerosol was almost completely volatile at 150°C. In the "clean" region, only the aerosol within the MBL was neutralized suggesting an oceanic source for any ammonia found in the particle phase. However, the FT continental plumes encountered during PEMT A and B were in general neutralized (most of the accumulation mode volume remained after heating to 150°C), implying the presence of ammonia in the particle phase even at high altitudes (far removed from the ocean surface). This fact and the presence of continental aerosol signatures (refractory aerosol, enhanced optical properties, etc.) imply an anthropogenic source for the inferred ammonium aerosol, consistent with observations from other experiments (INDOEX [*Ramanathan et al.*, 2001], SCAR-B [*Reid et al.*, 1998], and ASTEX [*Clarke et al.*, 1997]). This implication will be explored further in future research by the authors.

[83] The combustion component of the aerosol found within all the FT plumes showed the presence of refractory "cores"; this refractory constituent was inferred to be BC and was generally well mixed internally with the more volatile aerosol (within the FT combustion plumes). Other experiments also revealed internally mixed aerosol within continental emissions. Transmission Electron Microscopy (TEM) images revealed soot and sulfate/organic aerosols internally mixed within continental/combustion influenced air masses during INDOEX [*Ramanathan et al.*, 2001], ACE 1 [*Posfai et al.*, 1999], and SCAR-B [*Reid and Hobbs*, 1998; *Martins et al.*, 1998]. Thermal conditioning/volatility techniques coupled with size distribution instruments (similar to our volatility system) also indicated refractory aerosol internally mixed with more volatile components during INDOEX [*Ramanathan et al.*, 2001], SCAR-B [*Martins et al.*, 1998], and ASTEX [*Clarke et al.*, 1997].

[84] Gas phase and aerosol combustion indicators were generally linearly related within the plumes, but differences in these relationships were observed between the various regions. To what extent these differences were due to disparities in plume sources versus transport processes (convection, cloud processing, and scavenging) is not known at this time. Enhanced UF concentrations at or near horizontal and vertical plume boundaries were frequently observed, consistent with the earlier nucleation of new particles. This observation suggests that continental/combustion plume boundaries (when juxtaposed to "clean" air) may be a significant source of new particles in the FT.

[85] Relationships were also shown between various aerosol microphysical and optical properties. Submicron scattering and unheated volume were linearly related, revealing the link of scattering to aerosol mass loading. Absorption and submicron refractory volume were also proportional, confirming that a significant fraction of the refractory aerosol was BC. The ratio of refractory to unheated volume for the submicron component was nearly constant in all plumes at ~25%. However, the relationship of absorption and submicron refractory volume suggested that only 22% of the refractory volume was BC; therefore the ratio of submicron BC volume to submicron unheated (total) volume was 5.5%. Using appropriate densities (2.26 and 1.8 g/cm^3, for BC and sulfate aerosols, respectively), the ratio of BC to total accumulation mode mass would be ~7%. This is well in the range of values reported for other experiments that sampled continental/combustion emissions, including 14% in INDOEX [*Ramanathan et al.*, 2001], 5% in TARFOX [*Novakov et al.*, 1997], 5–20% in SCAR-B [*Artaxo et al.*, 1998; *Echalar et al.*, 1998; *Ross et al.*, 1998; *Martins et al.*, 1998; *Reid et al.*, 1998], 0.5–8.9% in TRACE A [*Pereira et al.*, 1996], and ~10% during SAFARI-92 [*Maenhaut et al.*, 1996].

[86] The discrepancy between submicron refractory volume (from OPC and DMA size distributions) and inferred BC volume (from PSAP/absorption) reveals a problem with the thermal conditioning/volatility approach to inferring size-resolved aerosol chemistry, especially in non-"clean" conditions. Namely, there are other submicron aerosol constituents present (especially in continental plumes) besides for the simplified system of sulfuric acid, sulfate, and BC aerosols normally considered in this type of analysis. Most notably, this approach cannot differentiate organic aerosols based on volatility, some of which are refractory and some of which are volatile.

[87] The radiatively important ω was ~0.88 for the PEMT A (biomass) FT plumes which would lead to a slight cooling of the combustion layer (depending on the underlying surface albedo, $\omega \leq 0.85$ leads to warming, higher values result in cooling [*Hansen et al.*, 1997]). The value of ω was much higher for the PEMT B (dust and pollution) FT plume at ~0.94. Most of this difference is attributable to the presence of the coarse mode dust; the submicron component of ω for this plume was in fact similar to the other regions at ~0.86. This similarity was due to the comparable fraction of refractory volume (proportional to absorption) to unheated volume (proportional to scattering) contained within the accumulation mode. The comparable value of ω (and refractory volume fraction) may represent a feature common for combustion plumes undergoing long-range transport in the remote marine FT.

[88] These values of submicron ω (combustion influenced) compare favorably to those determined for other experiments that sampled continental/combustion plumes. Values from INDOEX were determined to be ~0.9 [*Ramanathan et al.*, 2001] from a variety of different techniques. Values from TARFOX ranged between 0.89 and 0.93 [*Russell et al.*, 1999a, 1999b; *Hignett et al.*, 1999; *Hegg et al.*, 1997; *Novakov et al.*, 1997]. SCAR-B values ranged from 0.79 to 0.94 [*Eck et al.*, 1998; *Reid et al.*, 1998] with an average value near 0.87 [*Dubovik et al.*, 1998]. The average value for the accumulation mode ω reported for biomass burning aerosol plumes in the South Atlantic during TRACE A was ~0.85 [*Anderson et al.*, 1996a]. A global multiyear study [*Dubovik et al.*, 2002] utilizing ground-based radiometers from the AERONET network reported a range of ω values for both biomass burning (0.87–0.93) and urban/industrial aerosol (0.89–0.97). Differences in the values of ω are due to a variety of reasons, including measurement technique (in situ versus remote sensing), altitude range (column versus layer), RH effects ("dry" versus ambient), proximity to source (near source versus long-range transport), and aerosol type (biomass burning versus urban/industrial).

[89] The FT plumes encountered during PEMT A and B had lower values of ω than in the underlying MBL, even when the MBL was polluted. Lower ω values aloft suggest a greater BC concentration (and higher aerosol absorption relative to aerosol scattering). *Novakov et al.* [1997] reported an increase carbon mass fraction (percent of carbon mass to total submicron mass) with altitude during TARFOX. Layers with higher BC concentrations (and presumably higher absorption coefficients) than in the surface layer were observed during other experiments as well; however, this observation has not been sufficiently quantified to date. This implies that surface based in situ measurements may tend to overestimate ω (underestimate relative absorption) for the atmospheric column.

[90] **Acknowledgments.** This research was sponsored by the National Aeronautic and Space Administration's Global Tropospheric Experiment under grants NAG-1-1764 and NCC-1-315. We particularly appreciate the support of Joe McNeal, Jim Hoell, Jim Raper, and the GTE Project Office. Also, we would like to thank the University of Michigan (M. Carrol, G. Albercook, et al., PEMT A, ozone), UCAR/NCAR (B. Ridley et al., PEMT B, ozone), and NASA LARC (G. Sachse et al., PEMT A and B, CO) groups for the use of their measurements. Special thanks is also extended to the people of the NASA Wallops Island facility and the crew of the P3-B aircraft for their repeated assistance in accommodating our needs throughout both experiments. In addition, we would like to thank Mark Litchy and Barry Leinert for their help with instrumentation and programming issues.

References

Ackerman, A. S., O. B. Toon, D. E. Stevens, A. J. Heymsfield, V. Ramanathan, and E. J. Welton, Reduction of tropical cloudiness by soot, *Science*, *288*, 1042–1047, 2000.

Anderson, B. E., W. B. Grant, G. L. Gregory, E. V. Browell, J. E. Collins Jr., G. W. Sachse, D. R. Bagwell, C. H. Hudgins, D. R. Blake, and N. J. Blake, Aerosols from biomass burning over the tropical South Atlantic region: Distributions and impacts, *J. Geophys. Res.*, *101*, 24,117–24,137, 1996a.

Anderson, T. L., et al., Performance characteristics of a high sensitivity, three-wavelength, total scatter/backscatter nephelometer, *J. Atmos. Oceanic Technol.*, *13*, 967–986, 1996b.

Andreae, M. O., T. W. Andreae, R. J. Ferek, and H. Raemdonck, Long-range transport of soot carbon in the marine atmosphere, *Sci. Total Environ.*, *36*, 73–80, 1984.

Artaxo, P., E. T. Fernandes, J. V. Martins, M. A. Yamasoe, P. V. Hobbs, W. Maenhaut, K. M. Longo, and A. Castanho, Large-scale aerosol source apportionment in Amazonia, *J. Geophys. Res.*, *103*, 31,837–31,847, 1998.

Bates, T. S., B. J. Huebert, J. L. Gras, F. B. Griffiths, and P. A. Durkee, International Global Atmospheric Chemistry (IGAC) Project's First Aerosol Characterization Experiment (ACE 1): Overview, *J. Geophys. Res.*, *103*, 16,297–16,318, 1998.

Blake, N. J., et al., Influence of southern hemispheric biomass burning on midtropospheric distributions of nonmethane hydrocarbons and selected halocarbons over the remote South Pacific, *J. Geophys. Res.*, *104*, 16,213–16,232, 1999.

Bond, T. C., T. L. Anderson, and D. Campbell, Calibration and intercomparison of filter-based measurements of visible light absorption by aerosols, *Aerosol Sci. Technol.*, *30*, 582–600, 1999.

Charlson, R. J., J. Langner, H. Rodhe, C. B. Leovy, and S. G. Warren, Perturbation of the northern hemisphere radiative balance by backscattering from anthropogenic sulfate aerosols, *Tellus*, *43AB*, 152–163, 1991.

Chylek, P., G. Videen, D. Ngo, R. G. Pinnick, and J. D. Klett, Effect of black carbon on the optical properties and climate forcing of sulfate aerosols, *J. Geophys. Res.*, *100*, 16,325–16,332, 1995.

Clarke, A. D., Aerosol light absorption by soot in remote environments, *Aerosol Sci. Technol.*, *10*, 161–171, 1989.

Clarke, A. D., A thermo-optic technique for in situ analysis of size-resolved aerosol physicochemistry, *Atmos. Environ.*, *25*, 635–644, 1991.

Clarke, A. D., and J. N. Porter, Pacific marine aerosol, 2, Equatorial gradients in chlorophyll, ammonium, and excess sulfate during SAGA 3, *J. Geophys. Res.*, *98*, 16,997–17,010, 1993.

Clarke, A. D., K. J. Noone, J. Heintzenberg, S. G. Warren, and D. S. Covert, Aerosol light absorption measurement techniques: Analysis and intercomparisons, *Atmos. Environ.*, *21*, 1455–1465, 1987.

Clarke, A. D., T. Uehara, and J. N. Porter, Atmospheric nuclei and related aerosol fields over the Atlantic: Clean subsiding air and continental pollution during ASTEX, *J. Geophys. Res.*, *102*, 25,281–25,292, 1997.

Clarke, A. D., J. L. Varner, F. Eisele, R. L. Mauldin, D. Tanner, and M. Litchy, Particle production in the remote marine atmosphere: Cloud outflow and subsidence during ACE 1, *J. Geophys. Res.*, *103*, 16,397–16,409, 1998.

Clarke, A. D., F. Eisele, V. N. Kapustin, K. Moore, D. Tanner, L. Mauldin, M. Litchy, B. Lienert, M. A. Carroll, and G. Albercook, Nucleation in the equatorial free troposphere: Favorable environments during PEM-Tropics, *J. Geophys. Res.*, *104*, 5735–5744, 1999.

Clarke, A. D., W. G. Collins, P. J. Rasch, V. N. Kapustin, K. Moore, S. Howell, and H. E. Fuelberg, Dust and pollution transport on global scales: Aerosol measurements and model predictions, *J. Geophys. Res.*, *106*, 32,555–32,569, 2001.

Dibb, J. E., R. W. Talbot, E. M. Scheuer, D. R. Blake, N. J. Blake, G. L. Gregory, G. W. Sachse, and D. C. Thornton, Aerosol chemical composition and distribution during the Pacific Exploratory Mission (PEM) Tropics, *J. Geophys. Res.*, *104*, 5785–5800, 1999.

Dubovik, O., B. N. Holben, Y. J. Kaufman, M. Yamasoe, A. Smirnov, D. Tanre, and I. Slutsker, Single-scattering albedo of smoke retrieved from the sky radiance and solar transmittance measured from ground, *J. Geophys. Res.*, *103*, 31,903–31,923, 1998.

Dubovik, O., B. Holben, T. F. Eck, A. Smirnov, Y. J. Kaufman, M. D. King, D. Tanre, and I. Slutsker, Variability of absorption and optical properties of key aerosol types observed in worldwide locations, *J. Atmos. Sci.*, *59*, 590–608, 2002.

Echalar, F., P. Artaxo, J. V. Martins, M. Yamasoe, F. Gerab, W. Maenhaut, and B. Holben, Long-term monitoring of atmospheric aerosols in the Amazon Basin: Source identification and apportionment, *J. Geophys. Res.*, *103*, 31,849–31,864, 1998.

Eck, T. F., B. N. Holben, I. Slutsker, and A. Setzer, Measurements of irradiance attenuation and estimation of aerosol single scattering albedo for biomass burning aerosols in Amazonia, *J. Geophys. Res.*, *103*, 31,865–31,878, 1998.

Fishman, J., J. M. Hoell Jr., R. D. Bendura, R. J. McNeal, and V. W. J. H. Kirchoff, NASA GTE TRACE A experiment (September–October 1992): Overview, *J. Geophys. Res.*, *101*, 23,865–23,879, 1996.

Fuelberg, H. E., J. D. VanAusdall, E. V. Browell, and S. P. Longmore, Meteorological conditions associated with vertical distributions of aerosols off the west coast of Africa, *J. Geophys. Res.*, *101*, 24,105–24,115, 1996.

Fuelberg, H. E., R. E. Newell, S. P. Longmore, Y. Zhu, D. J. Westberg, and E. V. Browell, A meteorological overview of the PEM-TROPICS period, *J. Geophys. Res.*, *104*, 5585–5622, 1999.

Fuelberg, H. E., R. E. Newell, D. J. Westberg, J. C. Maloney, J. R. Hannan, B. D. Martin, M. A. Avery, and Y. Zhu, A meteorological overview of the second Pacific Exploratory Mission in the Tropics, *J. Geophys. Res.*, *106*, 32,427–32,443, 2001.

Fuller, K. A., W. C. Malm, and S. M. Kreidenweis, Effects of mixing on extinction by carbonaceous particles, *J. Geophys. Res.*, *104*, 15,941–15,954, 1999.

Gregory, G. L., D. J. Westberg, M. C. Shipham, D. R. Blake, R. E. Newell, R. W. Talbot, B. G. Heikes, G. W. Sasche, B. A. Anderson, and D. C. Thornton, Chemical characteristics of Pacific tropospheric air in the region of the ITCZ and SPCZ, *J. Geophys. Res.*, *104*, 5677–5696, 1999.

Hagen, D. E., M. B. Trueblood, and D. R. White, Hydration properties of combustion aerosols, *Aerosol Sci. Technol.*, *10*, 63–69, 1989.

Hansen, J., M. Sato, and R. Ruedy, Radiative forcing and climate response, *J. Geophys. Res.*, *102*, 6831–6864, 1997.

Hartley, W. S., P. V. Hobbs, J. L. Ross, P. B. Russell, and J. M. Livingston, Properties of aerosols aloft relevant to direct radiative forcing off the mid-Atlantic coast of the United States, *J. Geophys. Res.*, *105*, 9859–9885, 2000.

Hegg, D. A., J. Livingston, P. V. Hobbs, T. Novakov, and P. Russell, Chemical apportionment of aerosol column optical depth off the mid-Atlantic coast of the United States, *J. Geophys. Res.*, *102*, 25,293–25,303, 1997.

Heintzenberg, J., Size segregated measurements of particulate elemental carbon and light absorption at remote Arctic locations, *Atmos. Environ.*, *16*, 2461–2469, 1982.

Heintzenberg, J., R. J. Charlson, A. D. Clarke, C. Liousse, V. Ramaswamy, K. P. Shine, M. Wendisch, and G. Helas, Measurements and modelling of aerosol single-scattering albedo: Progress, problems and prospects, *Contrib. Atmos. Phys.*, *70*, 249–263, 1997.

Hignett, P., J. P. Taylor, P. N. Francis, and M. D. Glew, Comparison of observed and modeled direct aerosol forcing during TARFOX, *J. Geophys. Res.*, *104*, 2279–2287, 1999.

Hoell, J. M., et al., Pacific exploratory mission in the tropical Pacific: PEM-Tropics A, August–September 1996, *J. Geophys. Res.*, *104*, 5567–5584, 1999.

Hoppel, W. A., G. M. Frick, and R. E. Larson, Effect of non-precipitating clouds on the aerosol size distribution in the marine boundary layer, *Geophys. Res. Lett.*, *13*, 125–128, 1986.

Huebert, B. J., A. Pszenny, and B. Blomquist, The ASTEX/MAGE experiment, *J. Geophys. Res.*, *101*, 4319–4329, 1996.

Kaufman, Y. J., et al., Smoke, Clouds, and Radiation-Brazil (SCAR-B) experiment, *J. Geophys. Res.*, *103*, 31,783–31,808, 1998.

Kotchenruther, R. A., and P. V. Hobbs, Humidification factors of aerosols from biomass burning in Brazil, *J. Geophys. Res.*, *103*, 32,081–32,089, 1998.

Kotchenruther, R. A., P. V. Hobbs, and D. A. Hegg, Humidification factors for atmospheric aerosols off the mid-Atlantic coast of the United States, *J. Geophys. Res.*, *104*, 2239–2251, 1999.

Krishnamurti, T. N., M. C. Sinha, M. Kanamitsu, D. Oosterhof, H. Fuelberg, R. Chatfield, D. J. Jacob, and J. Logan, Passive tracer transport relevant to the TRACE A experiment, *J. Geophys. Res.*, *101*, 23,889–23,907, 1996.

Le Canut, P., M. O. Andreae, G. W. Harris, F. G. Wienhold, and T. Zenker, Airborne studies of emissions from savanna fires in southern Africa, 1, Aerosol emissions measured with a laser optical particle counter, *J. Geophys. Res.*, *101*, 23,615–23,630, 1996.

Lindesay, J. A., M. O. Andreae, J. G. Goldammer, G. Harris, H. J. Annegarn, M. Garstang, R. J. Scholes, and B. W. van Wilgen, International geosphere-biosphere programme/international global atmospheric chemistry SAFARI-92 field experiment: Background and overview, *J. Geophys. Res.*, *101*, 23,521–23,530, 1996.

Liousse, C., H. Cachier, and S. G. Jennings, Optical and thermal measurements of black carbon aerosol content in different environments: Variation of the specific attenuation cross-section, sigma (σ), *Atmos. Environ.*, *27*, 1203–1211, 1993.

Maenhaut, W., I. Salma, J. Cafmeyer, H. J. Annegarn, and M. O. Andreae, Regional atmospheric aerosol composition and sources in the eastern Transvaal, South Africa, and impact of biomass burning, *J. Geophys. Res.*, *101*, 23,631–23,650, 1996.

Martins, J. V., P. Artaxo, C. Liousse, J. S. Reid, P. V. Hobbs, and Y. J. Kaufman, Effects of black carbon content, particle size, and mixing on light absorption by aerosols from biomass burning in Brazil, *J. Geophys. Res.*, *103*, 32,041–32,050, 1998.

McCormick, M. P., P. H. Wang, and L. R. Poole, Stratospheric aerosols and clouds, in *Aerosol-Cloud-Climate Interactions*, edited by P. V. Hobbs, pp. 205–222, Academic, San Diego, Calif., 1993.

Novakov, T., D. A. Hegg, and P. V. Hobbs, Airborne measurements of carbonaceous aerosols on the East Coast of the United States, *J. Geophys. Res.*, *102*, 30,023–30,030, 1997.

NRC, Aerosol radiative forcing and climate change, *NRC Rep.*, pp. 26–34 and pp. 43–47, Natl. Acad. Press, Washington, D. C., 1996.

Penner, J. E., R. E. Dickinson, and C. A. O'Neill, Effects of aerosol from biomass burning on the global radiation budget, *Science*, *256*, 1424–1432, 1992.

Pereira, E. B., A. W. Setzer, F. Gerab, P. E. Artaxo, M. C. Pereira, and G. Monroe, Airborne measurements of aerosols from burning biomass in Brazil related to the TRACE A experiment, *J. Geophys. Res.*, *101*, 23,983–23,992, 1996.

Porter, J. N., A. D. Clarke, G. Ferry, and R. F. Penschel, Aircraft studies of size-dependent sampling through inlets, *J. Geophys. Res.*, *97*, 3815–3824, 1992.

Posfai, M., J. R. Anderson, P. R. Buseck, and H. Sievering, Soot and sulfate aerosol particles in the remote marine troposphere, *J. Geophys. Res.*, *104*, 21,685–21,693, 1999.

Raes, F., T. Bates, F. McGovern, and M. VanLiedekerke, The 2nd Aerosol Characterization Experiment (ACE 2): General overview and main results, *Tellus, Ser. B*, *52*, 111–125, 2000.

Ramanathan, V., et al., Indian Ocean Experiment: An integrated analysis of the climate forcing and effects of the great Indo-Asian haze, *J. Geophys. Res.*, *106*, 28,371–28,398, 2001.

Raper, J. L., M. M. Kleb, D. J. Jacob, D. D. Davis, R. E. Newell, H. E. Fuelberg, R. J. Bendura, J. M. Hoell, and R. J. McNeal, Pacific Exploratory Mission in the Tropical Pacific: PEM-Tropics B, March–April 1999, *J. Geophys. Res.*, *106*, 32,401–32,425, 2001.

Reid, J. S., and P. V. Hobbs, Physical and optical properties of young smoke from individual biomass fires in Brazil, *J. Geophys. Res.*, *103*, 32,013–32,030, 1998.

Reid, J. S., P. V. Hobbs, R. J. Ferek, D. R. Blake, J. V. Martins, M. R. Dunlap, and C. Liousse, Physical, chemical, and optical properties of regional hazes dominated by smoke in Brazil, *J. Geophys. Res.*, *103*, 32,059–32,080, 1998.

Remer, L. A., Y. J. Kaufman, and B. N. Holben, Interannual variation of ambient aerosol characteristics on the east coast of the United States, *J. Geophys. Res.*, *104*, 2223–2231, 1999.

Rosenfeld, D., TRMM Observed first direct evidence of smoke from forest fires inhibiting rainfall, *Science*, *26*, 3105–3108, 1999.

Ross, J. L., P. V. Hobbs, and B. Holben, Radiative characteristics of regional hazes dominated by smoke from biomass burning in Brazil: Closure tests and direct radiative forcing, *J. Geophys. Res.*, *103*, 31,925–31,941, 1998.

Russell, P. B., P. V. Hobbs, and L. L. Stowe, Aerosol properties and radiative effects in the United States East Coast haze plume: An overview of the Tropospheric Aerosol Radiative Forcing Observational Experiment (TARFOX), *J. Geophys. Res.*, *104*, 2213–2222, 1999a.

Russell, P. B., J. M. Livingston, P. Hignett, S. Kinne, J. Wong, A. Chien, R. Bergstrom, P. Durkee, and P. V. Hobbs, Aerosol-induced radiative flux changes off the United States mid-Atlantic coast: Comparison of values calculated from sun photometer and in situ data with those measured by airborne pyranometer, *J. Geophys. Res.*, *104*, 2289–2307, 1999b.

Schnell, R. C., Arctic haze and the arctic gas and aerosol sampling program (AGASP), *Geophys. Res. Lett.*, *11*, 361–364, 1984.

Smith, M. H., and C. D. O'Dowd, Observations of accumulation mode aerosol composition and soot carbon concentrations by means of a high-temperature volatility technique, *J. Geophys. Res.*, *101*, 19,583–19,591, 1996.

Stoller, P., et al., Measurements of atmospheric layers from the NASA DC-8 and P-3B aircraft during PEM-Tropics A, *J. Geophys. Res.*, *104*, 5745–5764, 1999.

Talbot, R. W., et al., Influence of biomass combustion emissions on the distribution of acidic trace gases over the southern Pacific basin during austral springtime, *J. Geophys. Res.*, *104*, 5623–5634, 1999.

Tang, I. N., and R. H. Munkelwitz, Composition and temperature dependence of the deliquescence properties of hygroscopic aerosols, *Atmos. Environ., Part A*, *27*, 467–473, 1993.

Thornton, D. C., A. R. Bandy, B. W. Blomquist, A. R. Driedger, and T. P. Wade, Sulfur dioxide distribution over the Pacific Ocean 1991–1996, *J. Geophys. Res.*, *104*, 5845–5854, 1999.

Twomey, S., M. Piepgrass, and T. L. Wolfe, An assessment of the impact of pollution on global cloud albedo, *Tellus, Ser. B.*, *36*, 356–366, 1984.

Waggoner, A. P., R. E. Weiss, N. C. Ahlquist, D. S. Covert, S. Will, and R. J. Charlson, Optical characteristics of atmospheric aerosols, *Atmos. Environ.*, *15*, 1891–1909, 1981.

Zhang, S. H., Y. Akutsu, L. M. Russel, R. C. Flagan, and J. H. Seinfeld, Radial differential mobility analyzer, *Aerosol Sci. Technol.*, *23*, 357–371, 1995.

A. D. Clarke, S. G. Howell, V. N. Kapustin, and K. G. Moore II, School of Ocean and Earth Sciences and Technology, University of Hawaii, Honolulu, HI, USA. (kmoore@soest.hawaii.edu)